MECHANICAL STRATIGRAPHY AND FAULT ZONE DEFORMATION OF THE

AUSTIN CHALK IN TEN-MILE CREEK, DESOTO, TEXAS

by

PATRICK CARTER LEWIS

Bachelor of Science, 2020
Texas Tech University
Lubbock, Texas

Submitted to the Graduate Faculty of the
College of Science and Engineering
Texas Christian University in partial
fulfillment of the requirements for the
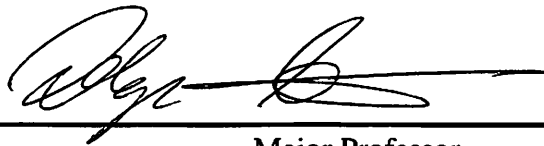degree of

Master of Science

December 2022

MECHANICAL STRATIGRAPHY AND FAULT ZONE DEFORMATION OF THE AUSTIN CHALK IN TEN-MILE CREEK, DESOTO, TEXAS
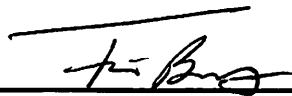
by

Patrick Carter Lewis

Thesis approved:

_____
Major Professor

_____

_____   Bs Herll 29 Nov '22

_____
For The College of Science and Engineering

ACKNOWLEDGEMENTS

Firstly, I would like to sincerely thank my family for their love and support in my journey

through higher education. Without their patience and endless confidence in me, I would not

be who I am today. I would like to express my gratitude and admiration for my thesis

advisor, Dr. Helge Alsleben, whose knowledge, experience, and encouragement has allowed

me to complete my research and studies. I would also like to acknowledge and thank my

committee members, Dr. Richard Denne and Bo Henk for their invaluable contributions. I

would also like to thank TCU geology faculty and staff for creating a welcoming

environment and providing me with the opportunity to further my pursuit in geosciences. I

would like to acknowledge my fellow graduate students for their support, friendship, and

camaraderie. Lastly, I would like to thank all those who completed previous studies used in

my research, without which I would not have the necessary foundation and knowledge to see

my research to completion.

TABLE OF CONTENTS

LIST OF FIGURES

LIST OF TABLES

Introduction

Deformation features in fine-grained sedimentary strata, including calcareous mudstone and chalk, are increasingly being seen as important to the development of unconventional and self-sourced oil and gas reservoirs (Ferrill et al., 2017a; Gillespie et al., 2021). The characterization of fractured reservoirs requires a detailed understanding of the geological history, as well as the rheological properties of the host rock (Gillespie et al., 2021). Faults are commonly the largest fractures in a fracture network, and form the backbone permeability systems in low permeability rocks (Ferrill et al., 2020). Horizontal drilling is often oriented perpendicular to fracture/fault networks to maximize production in naturally and/or hydraulically fractured reservoirs, but requires information on the orientation, spacing, and connectivity of fractures so that drilling depth and orientation can be set for maximum productivity (Wiltschko et al., 1991; Friedman and McKiernan, 1995). Prior to drilling, this information must come from outcrops. Outcrop studies provide the most complete view of a lithological unit or package of units, and are often the only way to view a rock unit in three dimensions.

Fracture patterns in outcrop are often more complex than their associated subsurface fracture network due to unloading during uplift and weathering at the surface. Despite increased complexity, previous research has shown that fracture parameters can be extrapolated to the subsurface with reasonable accuracy (Corbett et al., 1987; Wiltschko et al., 1991; Friedman and McKiernan, 1995). Because of the sampling biases associated with core data, well logs, and seismic data, outcrop studies remain the best method for characterizing deformation features of a lithological unit (Zeeb et al., 2013).

The Austin Chalk has historically been exploited as a conventional reservoir produced from natural, fracture related porosity and permeability without large hydraulic stimulations (Corbett et al., 1987; Ferrill et al., 2020). Conventional drilling activity peaked with discovery of prolific oil production in the Giddings field, Lee and Burleson Counties, Texas. The key to success in conventional plays has been to predict where natural fracturing is abundant (Corbett et al., 1987). The Austin Chalk is now being explored as a hybrid unconventional reservoir, relying on natural porosity and permeability combined with induced hydraulic fracturing to generate new fracture permeability to release hydrocarbons trapped in microscopic pores (Wiltschko et al., 1991; Callarotti and Millican, 2012; Ferrill et al., 2020).

Background

I.   Mechanical Stratigraphy

Mechanical stratigraphy is the practice of dividing rock strata into mechanical layers based on their material properties (e.g., hardness, compressive or tensile strength, Young's modulus), as well as the measure of the thickness of mechanical layers, and the characterization of the properties of the transitions between mechanical layers (e.g., friction) (Ferrill et al., 2017b). Mechanical stratigraphy is used to describe or model how a heterolithic sequence of rock units will deform under stress. This practice is not only useful in predicting deformation behavior, but is essential in understanding the deformation history of a formation.

Mechanical layering fundamentally controls carbonate fault zones (Ferrill and Morris, 2008). Mechanical stratigraphy influences fault nucleation, failure mode, displacement along

a fault zone, and damage zone characteristics (Ferrill et al., 2017b; Gillespie et al., 2021). Mechanical stratigraphy also affects fracture nucleation, fracture length, fracture spacing, aperture width, and the likelihood that a fracture will propagate across an interface (Helgeson and Ayton, 1991; Narr and Suppe, 1991; Ferrill et al., 2017a; b; McGinnis et al., 2017; Gillespie et al., 2021).

Mechanical stratigraphy is typically quantified using impact hammer devices. An impact hammer is a tool that records a hardness value when it strikes the surface of a material. The Schmidt hammer is an impact hammer tool that allows for a non-destructive method of evaluating bulk rock hardness in terms of surface rebound hardness (Basu and Aydin, 2004). When the Schmidt hammer is pressed against a surface, a spring-loaded piston is automatically released onto a plunger. Rebound value is defined as the measure of the resistance of a surface to impact penetration of the plunger tip (Aydin and Basu, 2005). The rebound height of the piston is considered to be an index of surface hardness (Basu and Aydin, 2004). Although the Schmidt hammer is very useful for outcrop studies, the applied force typically breaks subsurface core. To analyze the latter, the Proceq Equotip Bambino, which is a portable micro-rebound hammer for estimating hardness of rock material, is very useful (Verwaal and Mulder, 1993; Zahm and Enderlin, 2010; McClave, 2014).

II.   Geological Setting

The Austin Chalk is Upper Cretaceous, ranging from the base of Coniacian to the top of Lower Campanian (Larson et al., 1995; Hancock and Walaszczyk, 2004; Gale et al., 2008; Phelps et al., 2014) and represents deposition along a carbonate platform, platform edge, and deep-water shelf during a global eustatic sea-level highstand (Dravis, 1980; Hovorka and

Nance, 1994; Phelps et al., 2014). The Austin Chalk was deposited along the northern boundary of the Gulf of Mexico basin, a passive margin with a broad zone of transitional crust (Galloway, 2008; Cooper et al., 2020). Stratigraphically, the Austin Chalk lies unconformably above the Eagle Ford Shale, and is overlain by Cretaceous volcanic mounds and the Taylor Group (Figure 1). In the study area, the Austin Chalk is divided into three members; the lower Atco Member, the marl-rich Bruceville Member, and the upper Hutchins Member. The lower and upper members are predominantly massive bedded chalk deposits, whereas the middle Bruceville Member is a characteristic rhythmic limestone-marl sequence (Corbett et al., 1987). In North Texas, the Austin Chalk ranges in thickness from approximately 137 m (450 ft) to 168 m (550 ft) (Hovorka and Nance, 1994; Larson et al., 1995). Based on well logs taken from Dallas County, the Atco Member is approximately 55 m (180 ft) thick, and the Bruceville Member is up to 61 m (200 ft) thick in the study area (Larson et al., 1995). In addition to clay-rich marl units, the Austin Chalk contains several volcanic ash beds.
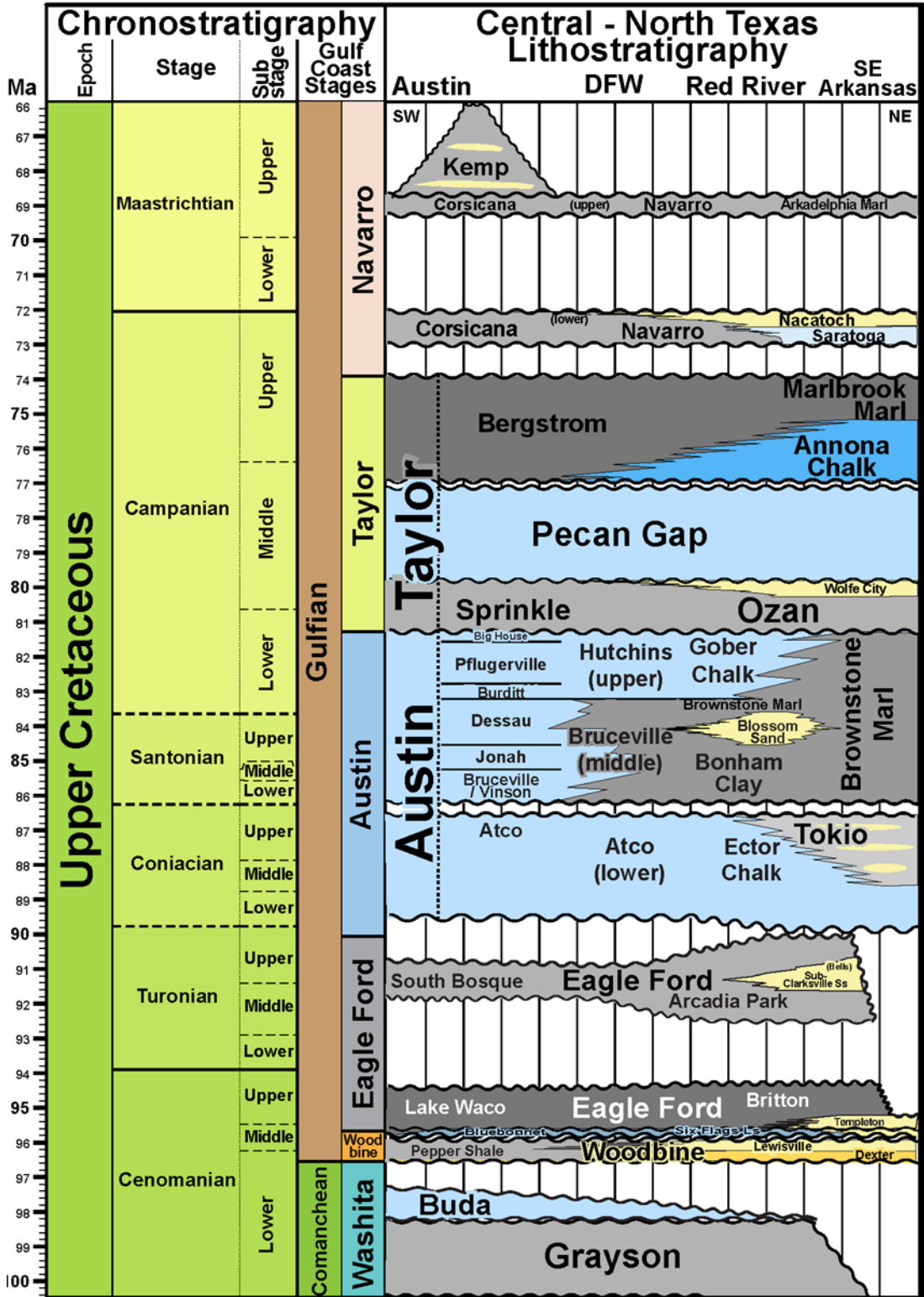
Figure 1: Columnar sections of Upper Cretaceous stratigraphic units in southern and eastern Texas. From Denne (2021, unpublished).

During the Coniacian, the depositional style in the Texas Shelf changed from the siliciclastic rich Eagle Ford Shale to the carbonate dominated Austin Chalk (Larson et al., 1995; Galloway, 2008; Phelps et al., 2014). The northwest Gulf remained an open platform connecting to the Cretaceous Western Interior Seaway, a shallow sea that covered the interior of North America (Figure 2). The Austin Chalk represents pelagic to hemipelagic deposits, characterized by the accumulation of open-shelf carbonates across the northwestern Gulf. Biostratigraphic evidence suggests the Austin depositional episode also records a shoaling cycle bounded by periods of deep water (Larson et al., 1995; Lundquist, 2000). During the Upper Cretaceous, periods of high sea-level and marine transgression restricted the influx of clastic sediment into the seaway and allowed for the deposition of a variety of carbonates (Longman et al., 1998; Galloway, 2008; Phelps et al., 2014). A "true" chalk is defined as a firm rock consisting of 60–100% microfossils, typically coccoliths and planktonic foraminifera (Denne, 2018). The Austin Chalk is a rhythmically bedded hemipelagic chalk with a variable clay content of 5-30% (Corbett et al., 1987), which may account for its very low porosity compared to most chalk deposits. The clay in the Austin Chalk is most likely volcanic in origin. Clay in the Bruceville Member coats microfossil grains, suggesting it is authigenic clay formed through the weathering of volcanic ash deposited with the chalk (Dravis, 1980; Hovorka and Nance, 1994). Tuffs and bentonites within the Austin most likely record volcanism related to the Western Cordillera and possibly volcanism related to southern Arkansas and on the Monroe Uplift (Collins, 1997; Galloway, 2008). Rhythmically deposited limestone-marl sequences are characteristic of the Cretaceous Western Interior Seaway and represent climatic changes that occurred during the Cretaceous (Eldrett et al., 2015). Multidisciplinary studies have hypothesized that the driving mechanisms for

rhythmically bedded strata are input of terrigenous sediments, intensity of bottom currents,

benthic oxygenation, and astronomical forces, rather than dramatic changes in sea level

(Damholt and Surlyk, 2004; Eldrett et al., 2015). The Campanian marks the renewal of

terrigenous sediment influx with the deposition of the overlying Taylor Group (Galloway,

2008).
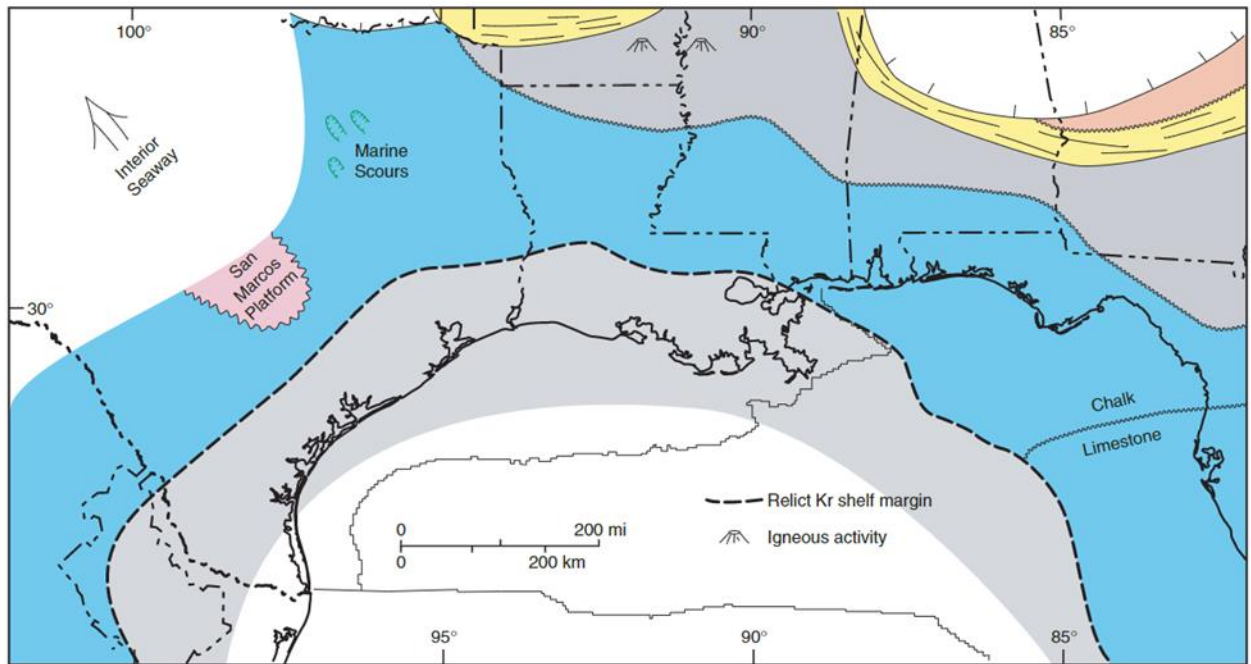
Figure 2: Paleogeography and depositional systems of the Northern Gulf of Mexico basin during the
Austin depositional episode. Taken from Galloway (2008).

The Balcones fault system cuts and juxtaposes rocks of the Cretaceous carbonate

platform section (Weeks, 1945; Ferrill and Morris, 2008). The fault system trends roughly

east-west at Del Rio, Texas and changes directions east of San Antonio and Austin. The fault

zone curves northward until it trends roughly north–south and terminates near Dallas, Texas,

and is coincident with the Cretaceous outcrop belt of Central Texas (Weeks, 1945; Reaser,

1961; Reaser and Collins, 1988; Ferrill and Morris, 2008) (Figure 3). The Balcones fault

system consists principally of normal faults dipping towards the southeast, although faults dip to the east near Dallas and to the south near Del Rio. Conjugate faults dipping towards the northwest are also observed (Reaser and Collins, 1988). The structural style of the Balcones is characterized by en echelon normal faults with many overlapping features such as relay ramps and horst bridges (Collins, 1993). Mosaics of closely spaced fractures occur in close proximity to faults and fault overlapping areas (Collins, 1993; Ferrill et al., 2011). Normal faults in the Balcones fault system provide important analogs for fault zone architecture and deformation in carbonate reservoirs worldwide (Ferrill and Morris, 2008). The pattern of faulting in the Balcones fault system is compatible with having formed in a relatively uniform normal faulting stress field, controlled by vertical maximum principal stress and horizontal minimum stress perpendicular to the fault trend (Ferrill and Morris, 2008). The Balcones trend is coincident with that of the subsurface Ouachita orogen through the region (Weeks, 1945; Wiltschko et al., 1991) and corresponds to the limit of normal faulting along the northwestern limit of the Gulf of Mexico Basin. Movement along the Balcones is thought to have occurred during the Miocene (Weeks, 1945; Galloway, 2008). Previous studies have concluded that the Austin Chalk has accommodated extensional deformation in the form of the Balcones fault system (Corbett et al., 1987; Wiltschko et al., 1991; Friedman and McKeirnan, 1995).
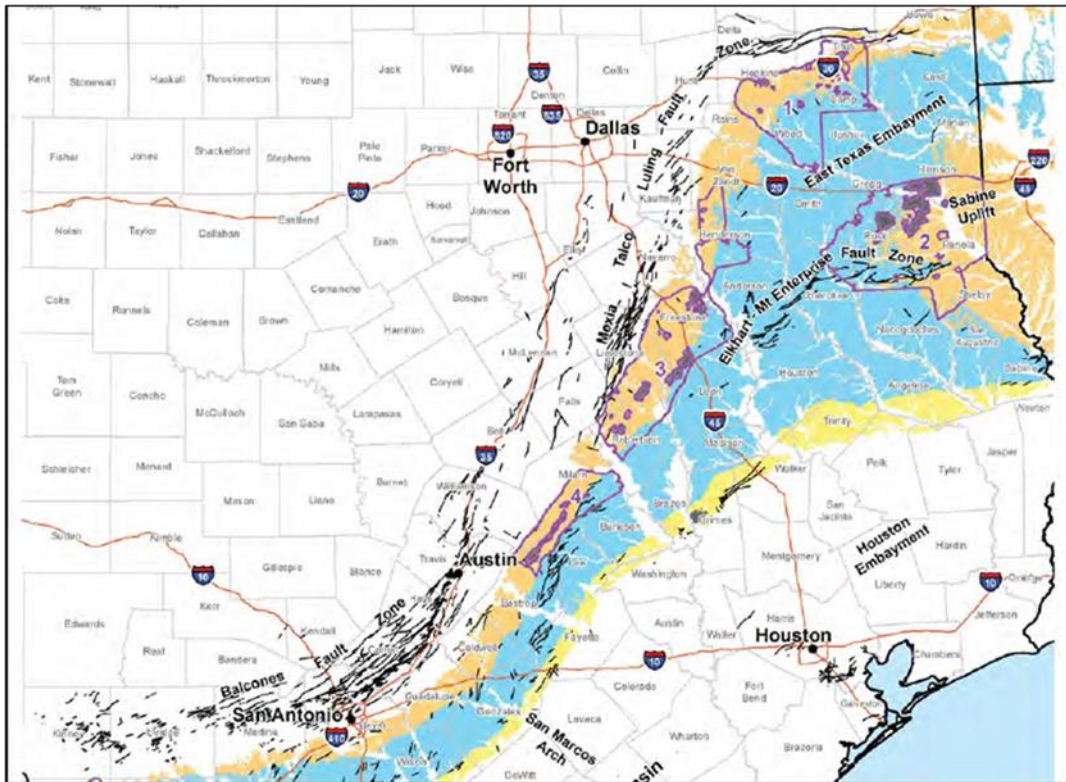
Figure 3: Map of Texas showing Balcones, and the Mexia-Talco-Luling Fault Trends, where black lines are faults, the blue shaded area is the Claiborne Group, yellow is the Jackson Group, and tan is the Wilcox Group. Taken from US Army Corps of Engineers Fort Worth District.

III.   Study Area

The study area includes two separate outcrops of the Austin Chalk in Dallas County, Texas (Figure 4). Outcrops are located in Ten-Mile Creek, which is a tributary of the Trinity River in DeSoto, Texas. The two sections of interest are informally named "the Church of the Nazarene" section and the "Walmart section" previously described by Gale et al. (2007). The Church of the Nazarene section can be accessed near a bridge near Ernie Robert's Park, where rhythmically bedded chalk and marl strata are near horizontal. Walking downsection, the strata become increasingly fractured, and become moderately dipping at a fault. The fault in this section of the creek is near the end of the exposed Cretaceous section. The Walmart

section is similar to the section described above. Near horizontal strata lead down section to a zone of fractured, folded, and faulted strata. Slickensided surfaces and calcite filled veins can be observed in abundance at this locality. This section can be followed until the strata return to near horizontal on both sides of the fault.

Previous studies on Ten-Mile Creek have focused primarily on biostratigraphy (Jacobson, 1961; Larson et al, 1995; Hancock and Walaszczyk, 2004; Gale et al., 2007) and geochemistry (Collins, 1997). The geology of Ten-Mile Creek was first described by researchers in the mapping department of Southern Methodist University (Williams, 1957; Ingles, 1959; Jacobson 1961). Williams (1957) and Jacobson (1961) both describe faulted sections within the chalk exposures in Ten-Mile Creek, but offer little in terms of structural analysis. The faults of Ten-Mile Creek were mapped by Ingles (1959) as a part of the Lancaster quadrangle. Previous efforts were compiled by Norton (1965) to produce a map of the surface geology of Dallas County (Figure 5).
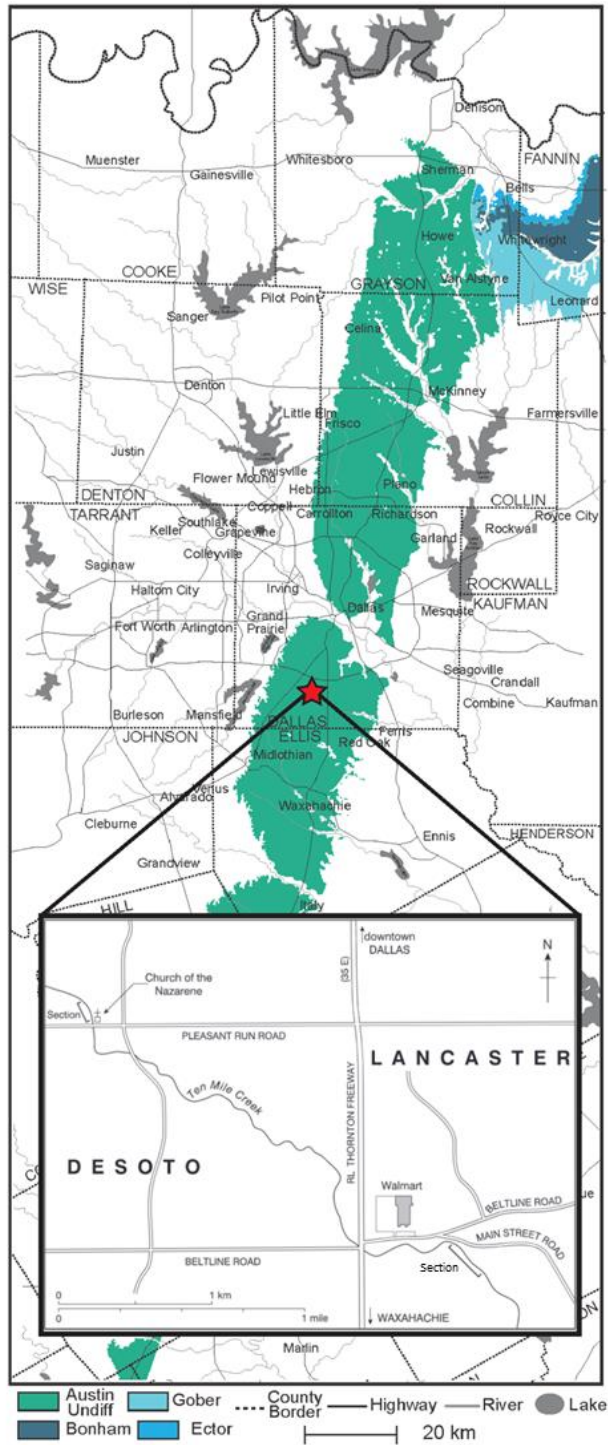
Figure 4: Map showing the outcrop trend of the Austin Chalk in north Texas. Red star denotes study area. Inset map of Ten-Mile Creek with Church of the Nazarene and Walmart sections shown. Inset map is modified from Gale et al. (2007).
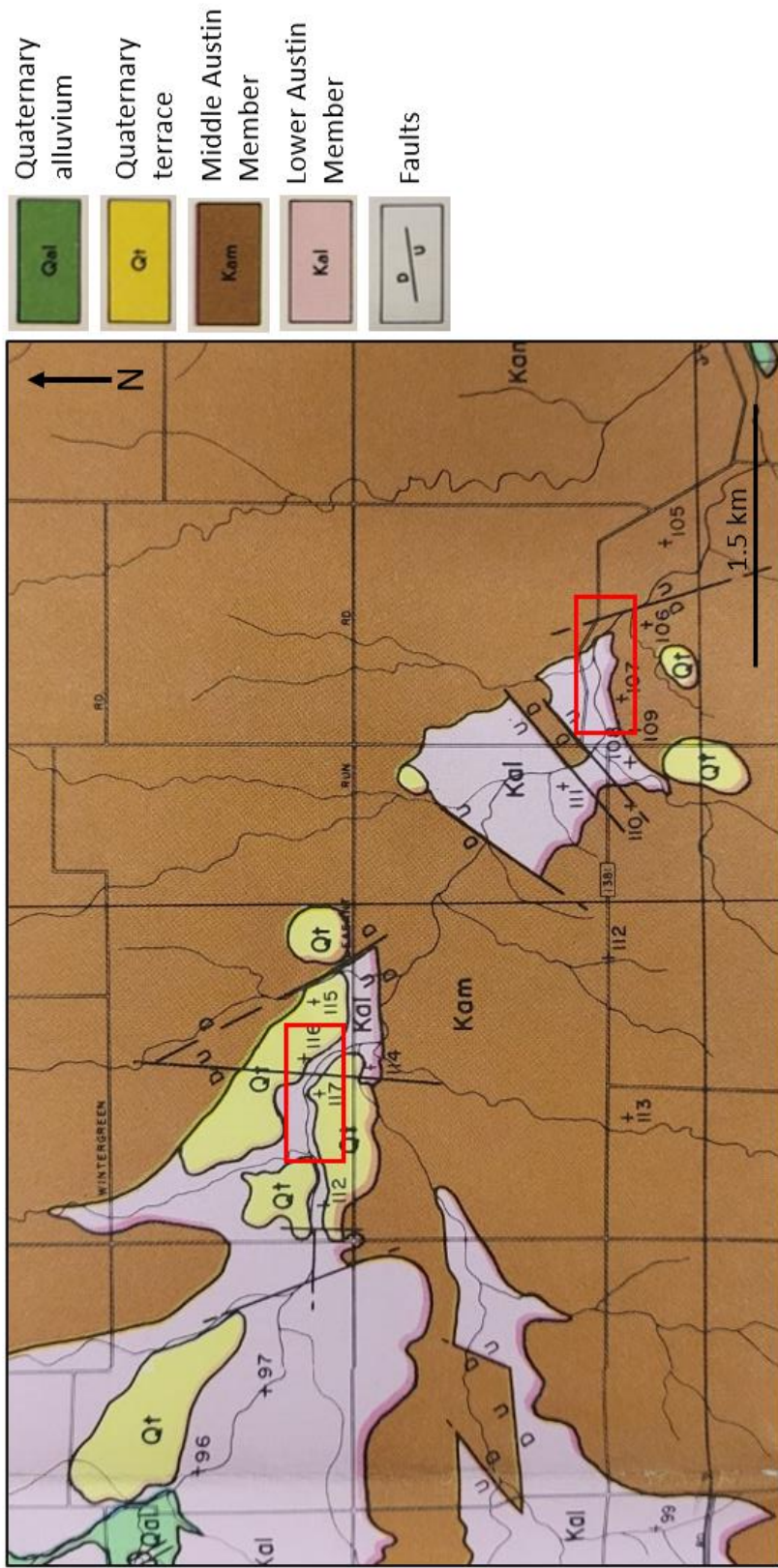
Figure 5: A portion of the geological map of Dallas County compiled by Norton (1965) showing Ten-Mile Creek. Outcrop sections shown in red rectangles.

Methodology

I.   Lithostratigraphy and Mechanical Stratigraphy

There are two sections present in outcrop in Ten-Mile Creek that are measured and described, the Church of the Nazarene section and the Walmart section. Measured sections are made using standard field tools including measuring tape and Jacob's staff. The rocks in the measured sections are identified as chalk, marly chalk, marl, calcareous mudstone, and bentonite lithologies. Lithological classification is based on Dunham's (1962) textural classification of carbonates and Loucks et al. (2020) lithofacies description of the Austin Chalk. Lithologies are determined qualitatively based on field observations.

The *in situ* mechanical properties of each lithostratigraphic layer in the sections are quantified using a type-N Schmidt hammer (Figure 6). The Schmidt hammer is a rebound hammer tool that provides a quick and relatively nondestructive measure of surface hardness that can be used to characterize mechanical properties of rock material (Basu and Aydin, 2004; Aydin and Basu, 2005; Bolla and Paronuzzi, 2021). Measurements in the field are made in the horizontal impact direction to reduce the effect of gravitational forces (Basu and Aydin, 2004; Aydin and Basu, 2005). Ten rebound measurements are made on each individual layer, and results are presented as average rebound value R. Lithologies that yield rebound measurements R<9 are not considered as this is the lowest value reliably measured by the type-N Schmidt hammer. Previous studies have shown that surface rebound values are sensitive to composition and clay content, and reflect the weathering profile of the measured section (Aydin and Basu, 2005; Ferrill et al., 2017a; 2017b; 2020).
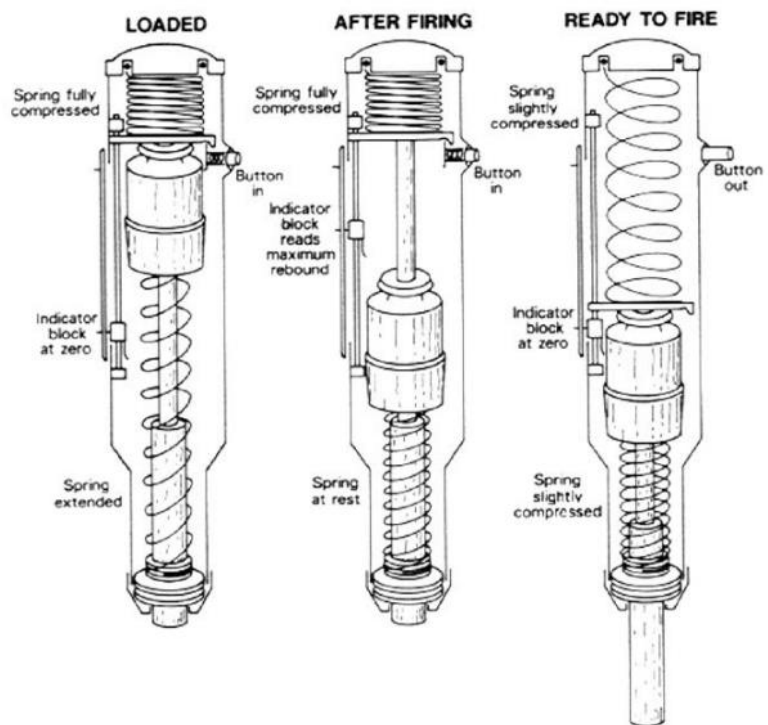
Figure 6: (Top) Type N Schmidt Hammer used in this study. (Bottom) Diagram of the working principle of the Schmidt Hammer. Taken from Basu and Aydin (2004).

II.   Gamma Ray

Gamma-ray measurements are made using a RS-230 spectrometer (Figure 7). The RS-230 spectrometer is a portable hand-held radiation spectrometer survey instrument used in the geophysical industry (Radiation Solutions Inc). The RS-230 provides a convenient and nondestructive method to measure the spectral gamma ray properties of rock material in outcrop. Measurements are made every six inches (~15 cm) through both the Church of the Nazarene section and Walmart section of Ten-Mile Creek. Results provide concentrations for Potassium (wt. percent), Uranium (ppm), and Thorium (ppm). Additionally, these values are used to calculate and produce a gamma ray API curve for the measured sections.

Figure 7: RS-230 handheld gamma ray reader (picture taken from Radiation Solutions Inc).

III. Linear Scanline Surveys

Fracture data is gathered in the field using linear scanline surveys (Figures 8 and 9). Scanline surveys provide a systematic method for measuring fracture attributes in the field that can be used to characterize fracture networks of a formation. Linear scanlines are created by forming a line on a bedding surface using a measuring tape, and attributes of each fracture that intersects the line are measured (Priest and Hudson, 1981). In this study, mechanically competent layers are chosen for scanlines. The orientation of fractures is measured using a Brunton compass, and the position of each fracture on the scanline is noted. Additionally, when possible, each fracture is characterized as either bed bound or non-bed bound. Scanline length and orientation are limited by the area of the outcrop surface. A total of seven linear scanline surveys ranging in 15 to 50 meters in length are performed on the outcrops present in Ten-Mile Creek. Linear fracture spacing, defined as spacing between fractures, and linear fracture intensity, defined as number of fractures per unit length, are presented for each scanline survey.

Linear scanlines are influenced by several forms of sampling bias (Lacazette, 1991; Zeeb et al., 2013; Watkins et al., 2015). Orientation bias is caused by fractures that intersect the scanline at oblique angles, and may result in overestimation of fracture spacing and an underestimation of fracture intensity. Orientation bias in fracture data is corrected using the method presented by Lacazette (1991). Truncation bias is caused by unavoidable resolution limitations (Zeeb et al., 2013). Limitations in outcrop size will cause censoring bias, and the underrepresentation of fractures of smaller lengths will cause size bias (Zeeb et al., 2013). Because fracture length is not considered in this study, there is no correction for censoring

and size bias. In addition to fracture surfaces, structural features such as slickensides and bedding surfaces are measured using a Brunton compass as well.
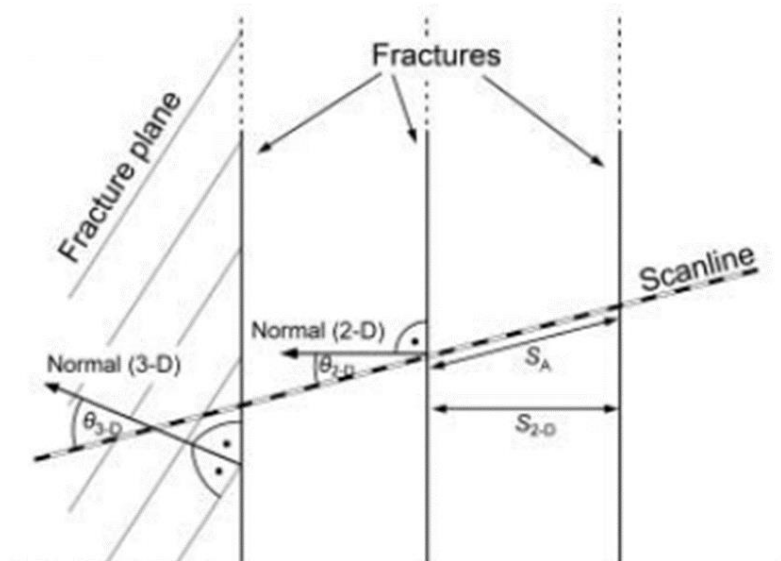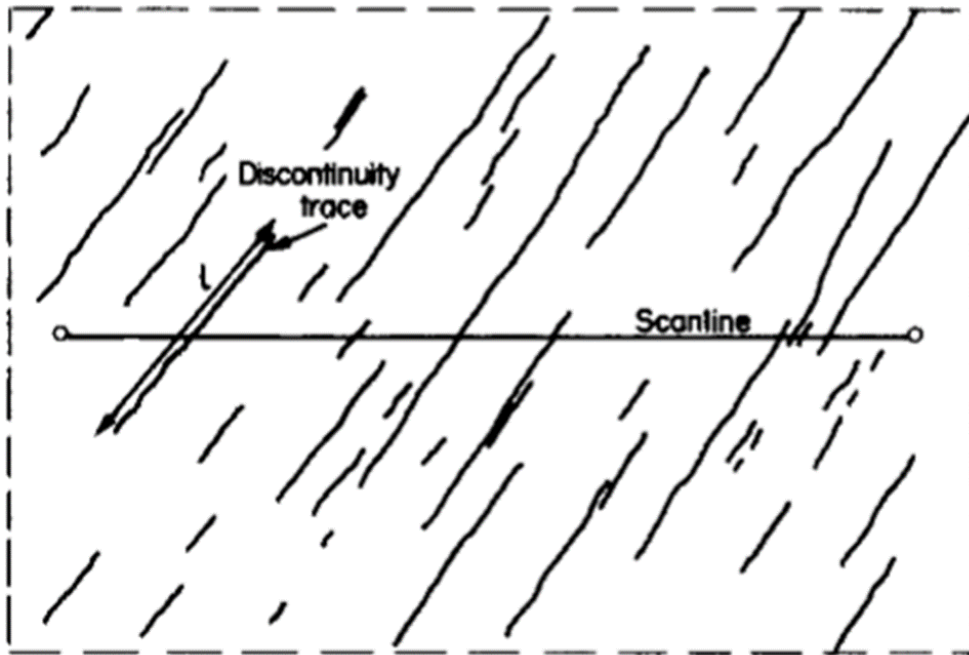
Figure 8: (Top) Diagram representation of a linear scanline intersecting a fracture set. Taken from Priest and Hudson (1981). (Bottom) Diagram illustrating orientation bias in fracture spacing measured from linear scanline surveys, and variables needed to correct for true spacing. S_A is the apparent spacing measured from the scanline. S_{2-D} is the true fracture spacing. Taken from Zeeb et al. (2013).

Figure 9: Example of a linear scanline on bedding surface in Walmart Section of Ten-Mile Creek.

Results

I.   Lithostratigraphy of Ten-Mile Creek

Five lithologies are observed across the two sections in Ten-Mile creek: chalk, marly

chalk, marl, calcareous mudstone, and bentonite (Figures 10-13). Chalk units are typically

the lightest in color and contain the highest relative abundance of carbonate. Marl units

appear gray in color and contain approximately 50% carbonate and 50% siliciclastic material.

Marly chalk serves as an intermediate designation between chalk and marl. Calcareous

mudstone units are dark grey and finely laminated. These units are prone to weathering and

contain a high relative abundance of siliciclastic material. Bentonite units are highly

recessive in outcrop and orange in color. These units represent volcanic ash layers in the

sections. Inoceramid and ammonites are locally present throughout the section, and shell lag

packstone layers are also observed. Slickensides with calcite mineralization and brecciated

gouge are observed in close proximity to faults (Figures 14 and 15). Numerous trace fossils

are observed in Ten-Mile Creek, including *Thalassinoides*, *Chondrites*, *Asterosoma*,

Planolites, *Rosselia*, *Paleophycus*, and *Skolithos*. Pyrite nodules 1 cm to 6 cm in diameter are

observed as well.

Figure 10: Outcrop photo from Ten-Mile Creek showing recessed, orange bentonite layer between layers of calcareous mudstone and chalk.

Figure 11: Outcrop photo from Ten-Mile Creek showing rhythmic sequence of chalk, marly chalk, and calcareous mudstone.

Figure 12: Outcrop photo from Ten-Mile Creek showing sequence of calcareous mudstone and thin chalk layers.

Figure 13: Photo showing typical, grey marl unit, with pronounced bioturbation near the top of the bed.

Figure 14: Slickensides with calcite mineralization.

Figure 15: Brecciated fault gouge from the fault core of the normal fault observed in the Church of the Nazarene section of Ten-Mile Creek.

The Church of the Nazarene measured section (Figures 16 and 17) begins at the lowest accessible stratigraphic unit (0 ft in measured section) and includes 18.3 m (60 ft) of Austin Chalk. A normal fault contact is observed within this section at 6.4 m (21 ft). The rocks in the hanging wall of this fault consist mostly of grey calcareous mudstone interlayered with thin beds of white to tan chalk and marly chalk. Calcareous mudstone units are subject to strong weathering and are typically slope forming units. Chalk and marly chalk lithologies are more resistant and stand out in weathering profile compared to calcareous mudstone. The rocks in the hanging wall section are highly fractured and gently (180°-120°) folded. Pyrite nodules are common in this interval. Numerous slickensides are observed with calcite mineralization near the main fault. These surfaces have an average orientation of 199°/65°, although numerous conjugate fracture surfaces are observed as well. The rocks in the footwall of the Church of the Nazarene exposure make up the remaining 12 m (39.5 ft) of the section, and consist of interbedded white chalk and grey marl units. Multiple grey to orange bentonite layers are observed, including a 15 cm (6 in) thick bentonite at 2.4 m (8 ft). Lithologic units in this portion are much more competent and resistant to weathering than those of the hanging wall (with the exception of bentonites). The footwall section is also less fractured than the hanging wall.

The Walmart measured section (Figures 18 and 19) begins at the lowest accessible stratigraphic unit (0 ft in measured section) and includes 24.7 m (81 ft) of Austin Chalk. The first 9 m (30 ft) of the measured section consists of interlayered chalk, marl, and calcareous mudstone. Bedding in this portion of the section is subhorizontal and contains mudstone layers 0.9 to 1.2 m (3 to 4 ft) thick. Two normal faults with approximate displacements ~1 m (3 ft) are observed in this section at 6.4 m (21 ft) and 8.5 m (28 ft). Lithologic layers in this

portion moderately dip 34° to the south-southeast, and are similar in lithology to the previous portion, although abundant jointing and pyrite nodules are recognized. Inoceramid fragments and thin fossiliferous packstone layers are also observed. Another normal fault contact is observed at 22.9 m (75 ft) in this section. Rocks in the footwall make up the remaining 1.8 m (6 ft) of the Walmart section, and consists predominantly of chalk and marly chalk. A single 10 cm (4 in) bentonite is observed at 23.1 m (76 ft). Numerous slickensides with calcite mineralization are observed in the Walmart section in addition to the faults noted. These surfaces have average orientations of 340°/63° and 166°/43°. Geological maps and cross sections are constructed for both the Church of the Nazarene and Walmart sections (Figures 20 and 21).
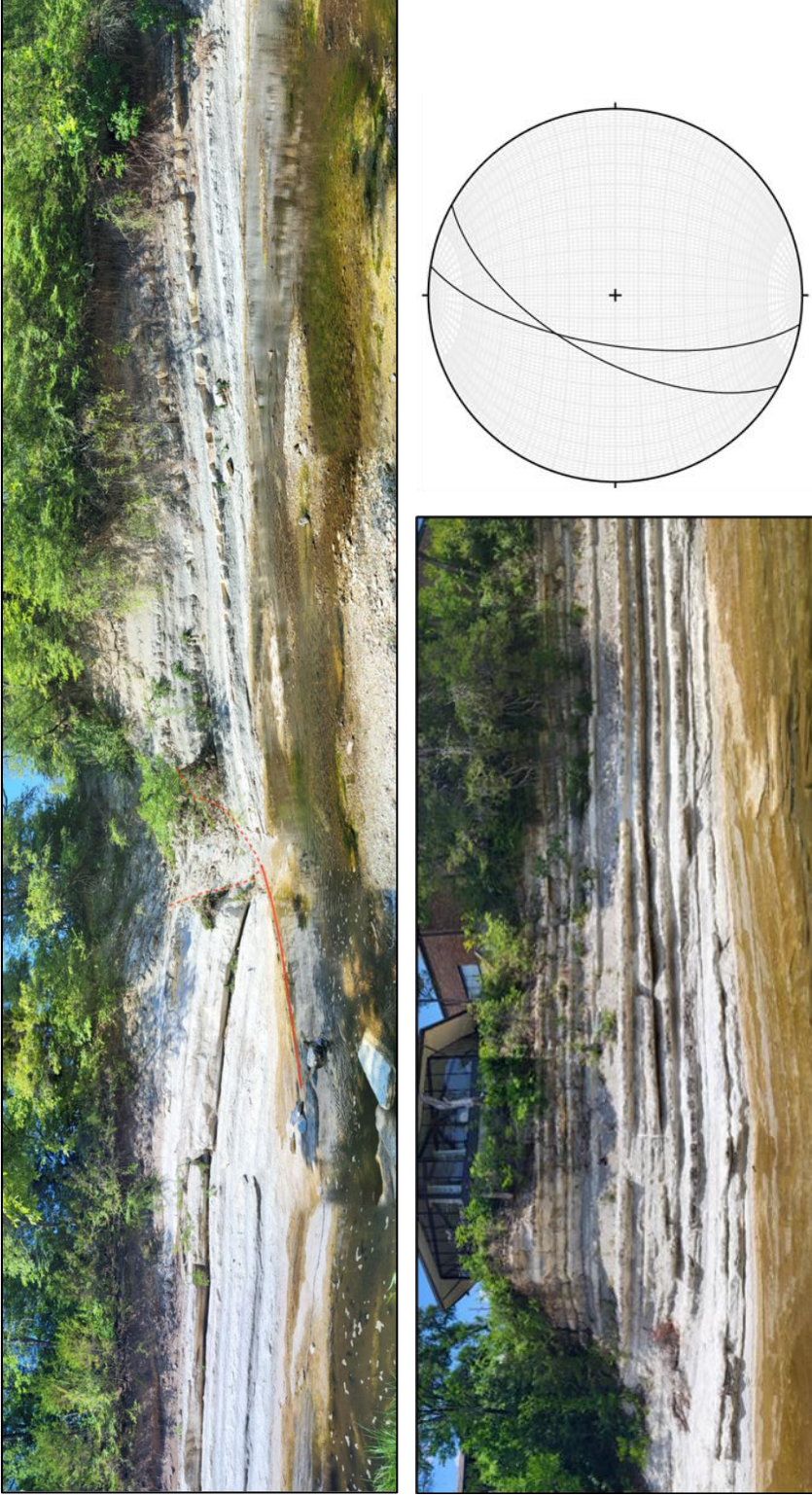
Figure 16: Photomosaics of outcrops in Church of the Nazarene section of Ten-Mile Creek. (Top) Facing southwest, fault damage zone, note folded strata and contrasting lithologies at fault contact. Trace of fault shown in red, note fault is partially obscured by gouge rock. (Bottom left) Facing northeast, relatively undeformed section of outcrop downstream of damage zone. (Bottom right) Lower hemisphere equal area stereographic projection of slickenside measurements from the Church of the Nazarene section of Ten-Mile Creek.
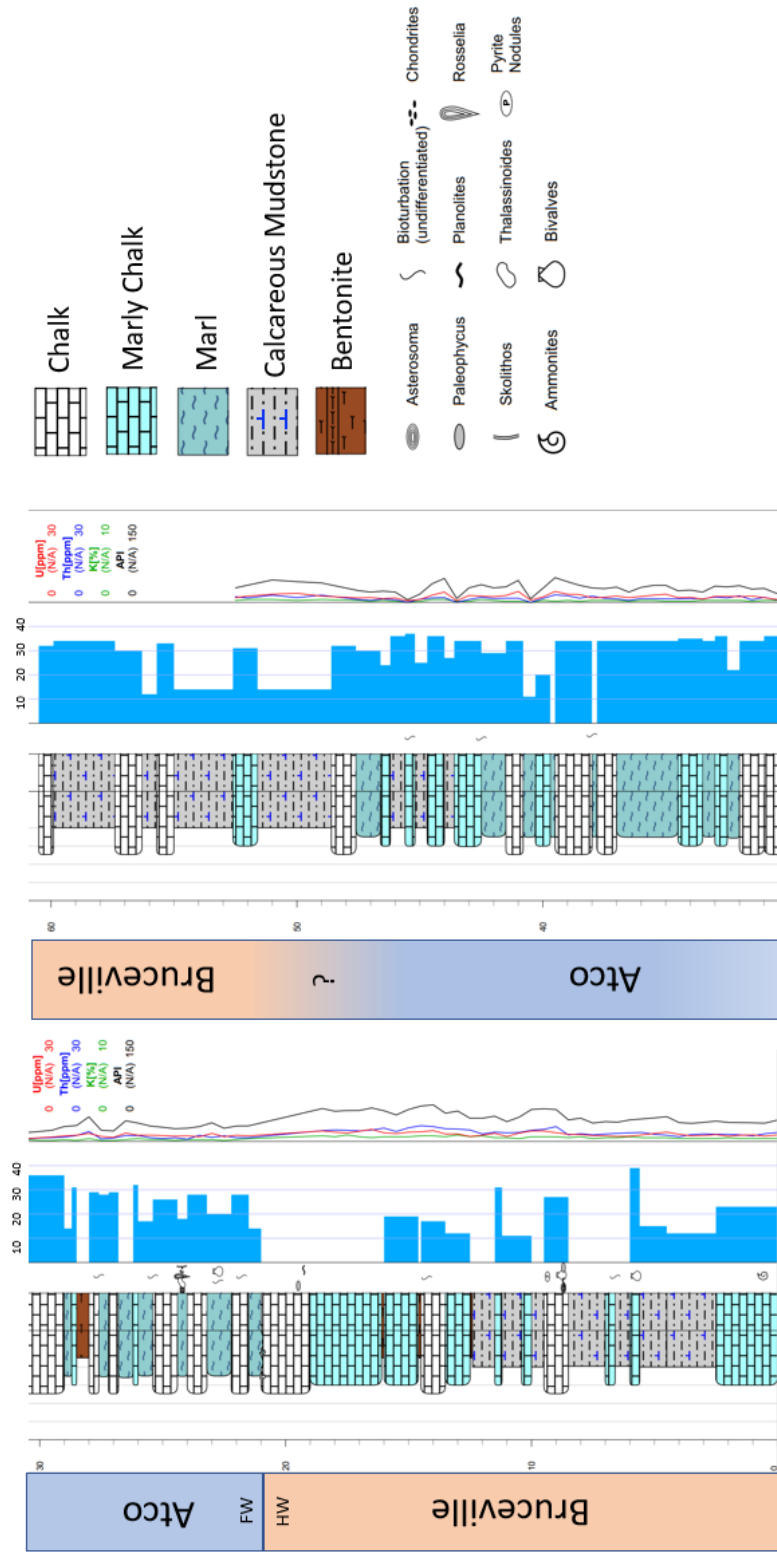
Figure 17: Lithostratigraphic, mechanical rebound, and spectral gamma ray profiles for the measured section of the Church of the Nazarene section of Ten-Mile Creek. Gaps in rebound profile are due to either the lithologic unit not yielding a reliable rebound value, or being physically out of reach in the field.
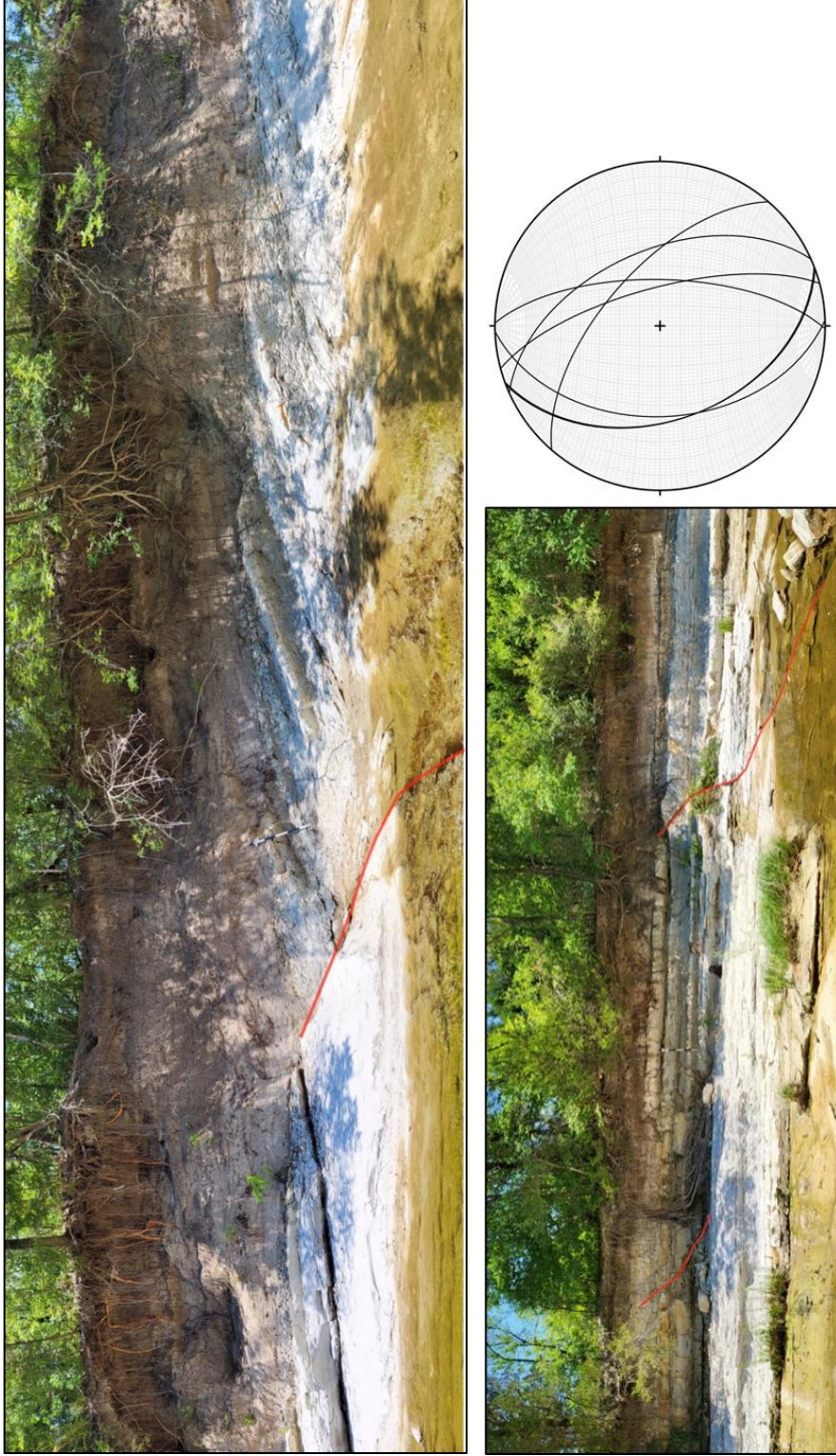
Figure 18: Photomosaics of outcrops in Walmart section of Ten-Mile Creek. 1.67 m (5.5 ft) Jacob's staff for scale. Fault trace shown in red. (Top) Facing southwest, normal fault contact at 22.9 meters, note tilted and highly fractured strata on northwest side of fault. (Bottom left) Facing northeast, subhorizontal section showing two faults with minimal offset at 6.4 and 8.5 meters. (Bottom right) Lower hemisphere equal area stereographic projection of slickenside measurements from the Walmart section of Ten-Mile Creek
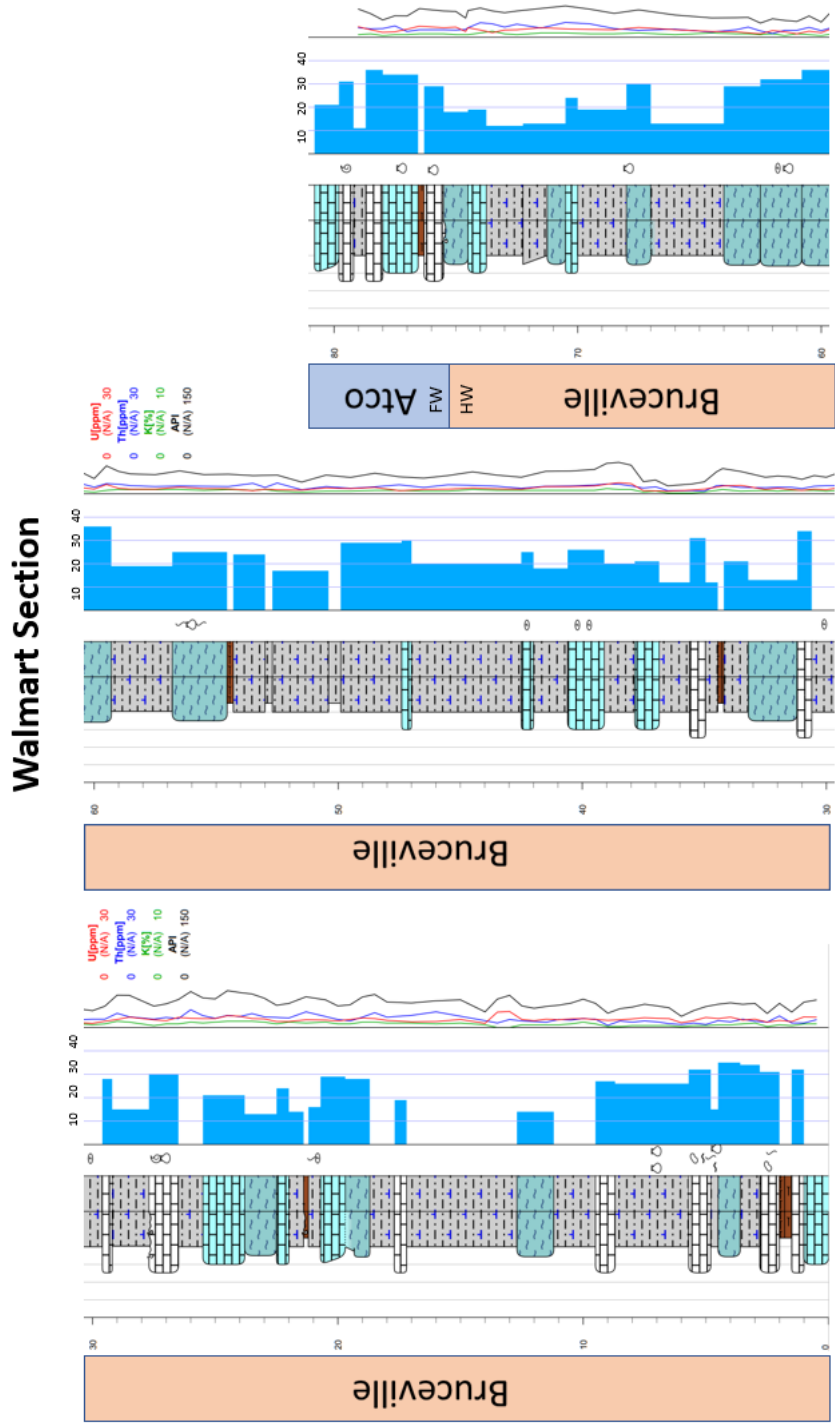
Figure 19: Lithostratigraphic, mechanical rebound, and spectral gamma ray profiles for the measured section of the Walmart section of Ten-Mile Creek. Gaps in rebound profile are due to either the lithologic unit not yielding a reliable rebound value, or being physically out of reach in the field.
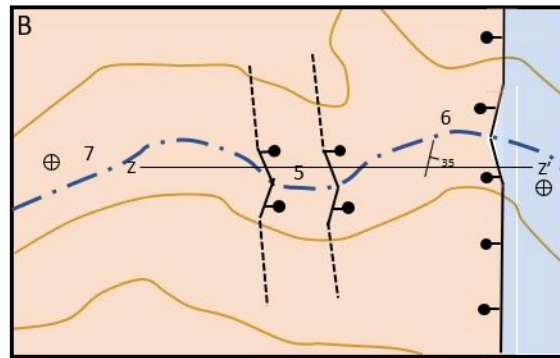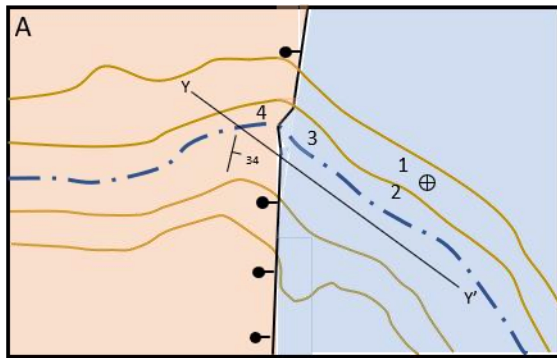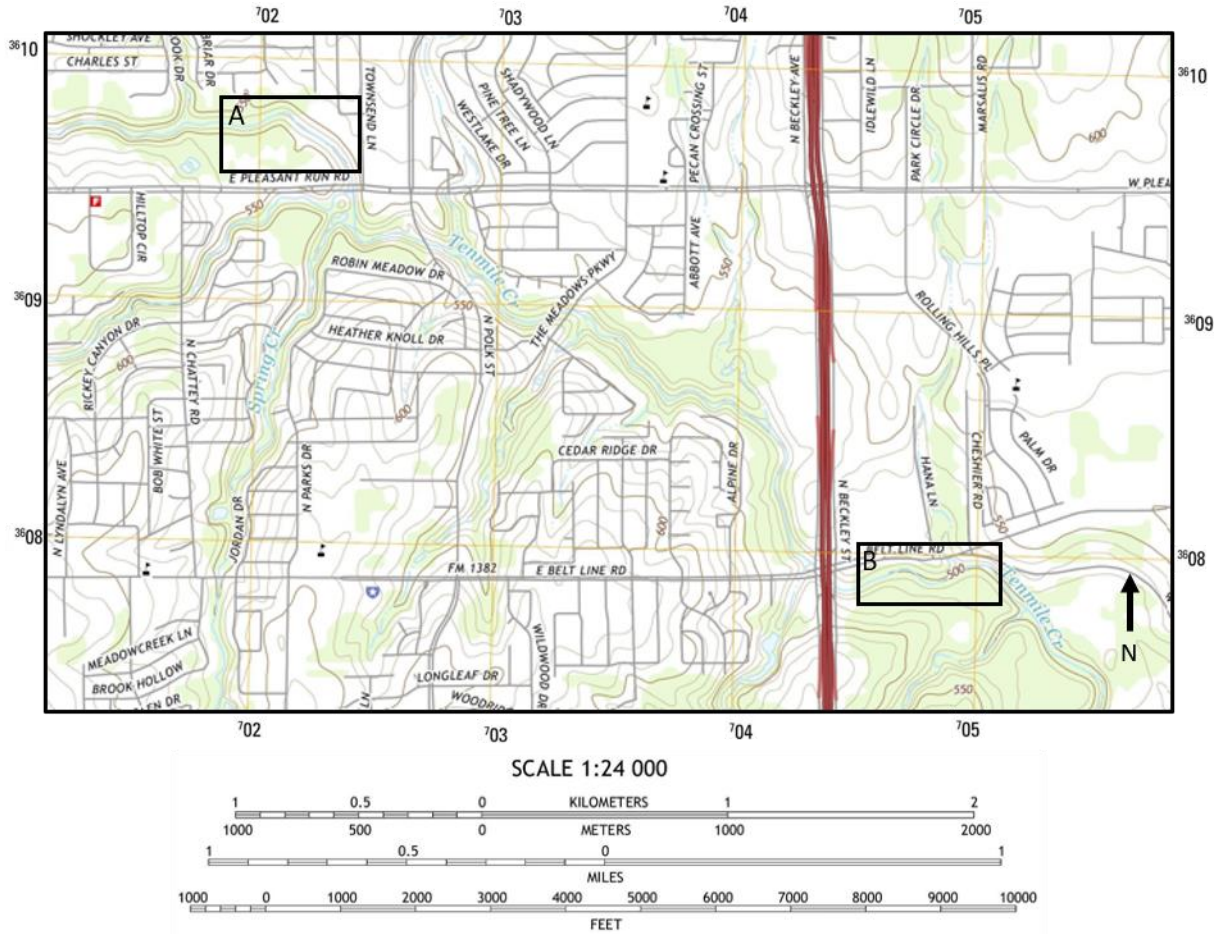
Figure 20: Geological maps of the Church of the Nazarene section (A) and Walmart section (B). Atco Member of the Austin Chalk shown in blue. Bruceville Member of the Austin Chalk shown in orange. Numbers indicate locations of linear scanline surveys.
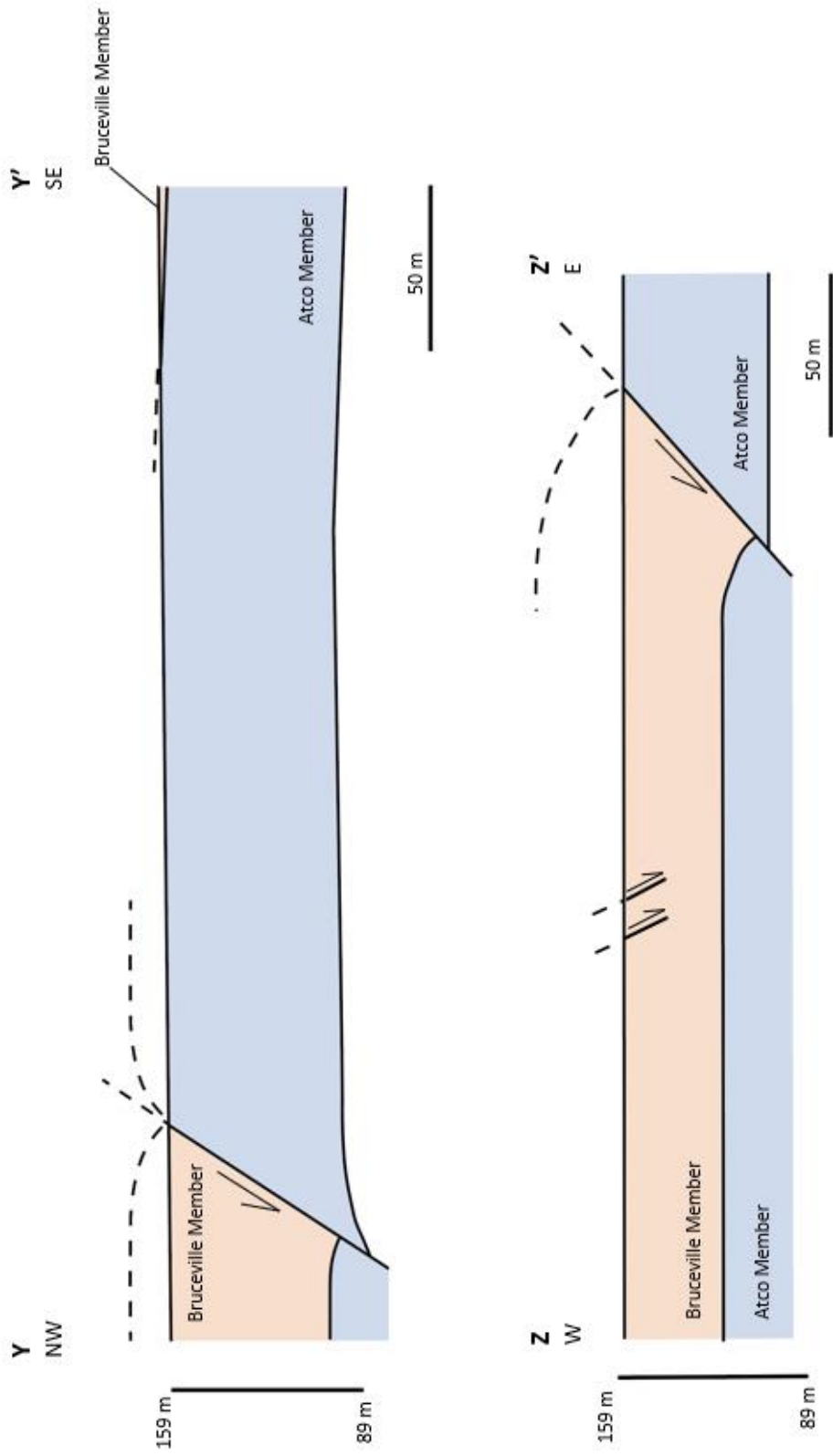
Figure 21: (Top) Cross-section through the Church of the Nazarene section of Ten-Mile Creek. (Bottom) Cross-section through the Walmart section of Ten-Mile Creek.

II.   Mechanical Stratigraphy

The Schmidt hammer rebound numbers (R) are used to construct a rebound profile for the Church of the Nazarene section and the Walmart section of Ten-Mile Creek (Figures 17 and 19). The rebound profiles show distinctive mechanical layering for both outcrop sections of Ten-Mile Creek, and reflect the weathering profile of the outcrop. In total, R values range from 9 to 35.9. Chalk lithologies form the most competent layers (average R values ranging from 16.79 to 35.9, and mean value of 29.13), and are the most resistant to weathering in outcrop. Marly chalk lithologies are of similar competency to chalk layers, but show a wider range in values (average R values ranging from 12 to 38.5, and mean value of 27.67). Marl lithologies are less competent than chalk lithologies, and show a similar range as, but lower mean than that of marly chalk (average R values ranging from 9.2 to 35.1, and mean value of 20.89). Calcareous mudstone lithologies form the least competent layers in outcrop (average R values ranging from 11 to 35.6, and mean value of 18.09), and are the most susceptible to weathering. Previous studies have concluded that rebound values are inversely correlated to clay content (Ferrill et al., 2011; McGinnis et al., 2017; Ferrill et al., 2020), as is qualitatively shown by the mean rebound values for each lithology. Mudstone layers of considerable thickness weather to slopes in outcrop, and thin mudstone layers form deep recesses between more competent layers. Rocks in the hanging wall of the Church of the Nazarene section are dominated by thick mudstone layers with occasional thin layers of more competent lithologies. By contrast, the rocks in the footwall are dominated by competent layers of chalk and marl. Near the top of the footwall the measured section transitions back to a zone of thick layers of calcareous mudstone.

Mechanically, the measured sections may be broken into sections that can be classified as weak (predominately R<20), intermediate (predominately R=20-30), and strong (predominately R>30). The rocks in the hanging wall of the Church of the Nazarene section are considered weak. The alternating sequence of chalk and marl in the lower section of the footwall is considered intermediate. The section from ~9 to 12 m (29 to 40 ft), which consists of thick chalk and marly chalk units, is considered the strongest portion of the section. The section transitions to a zone of intermediate strength, then the remaining 3 m (10 ft) of the section is classified as weak again. The majority of the Walmart section is classified as weak, with zones of intermediate strength at 0.6-1.8 m (2-6 ft) and 5.8-7.6 m (19-25 ft). The section from 18 to 20 m (59 to 65 ft) is considered strong, and the portion of the section above 22.9 m (75 ft) (footwall of the fault) is classified as strong.

R values for each mechanical layer are compared to mechanical layer thickness (cm) for each of the four lithologies (Figures 22 and 23). There is very little correlation between R and mechanical layer thickness. Only the chalk lithologies show a tight grouping in R values, whereas marly chalk, marl, and calcareous mudstone show considerable scatter. Although clay content was not quantified for strata in Ten-Mile Creek, results suggest that lithology has a much stronger influence over mechanical rebound value than mechanical layer thickness.
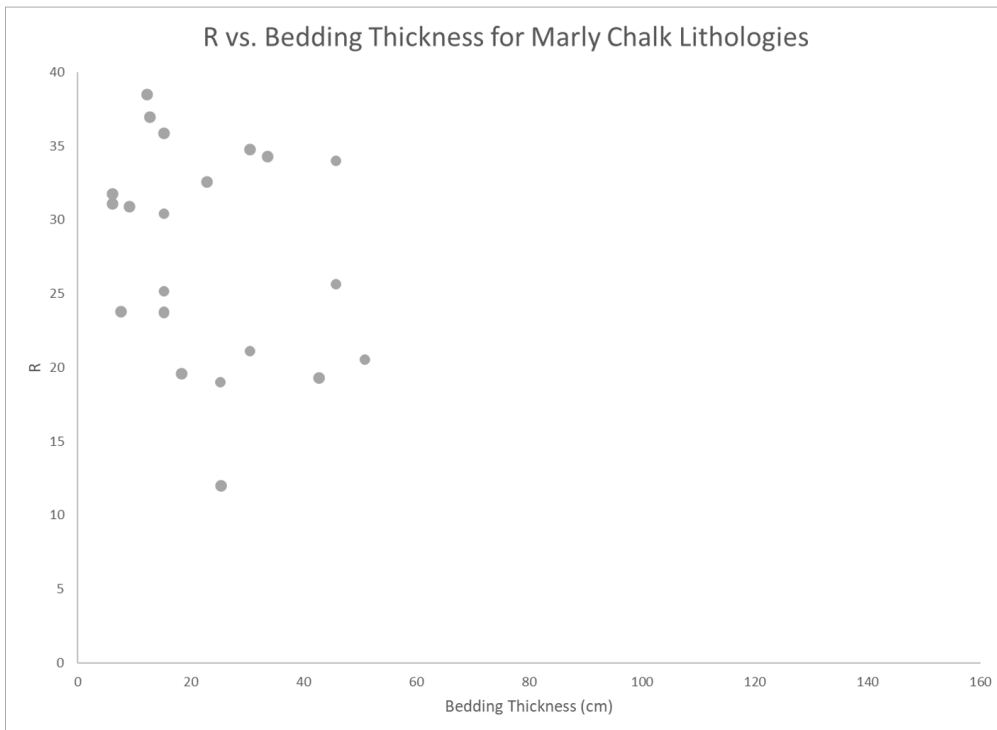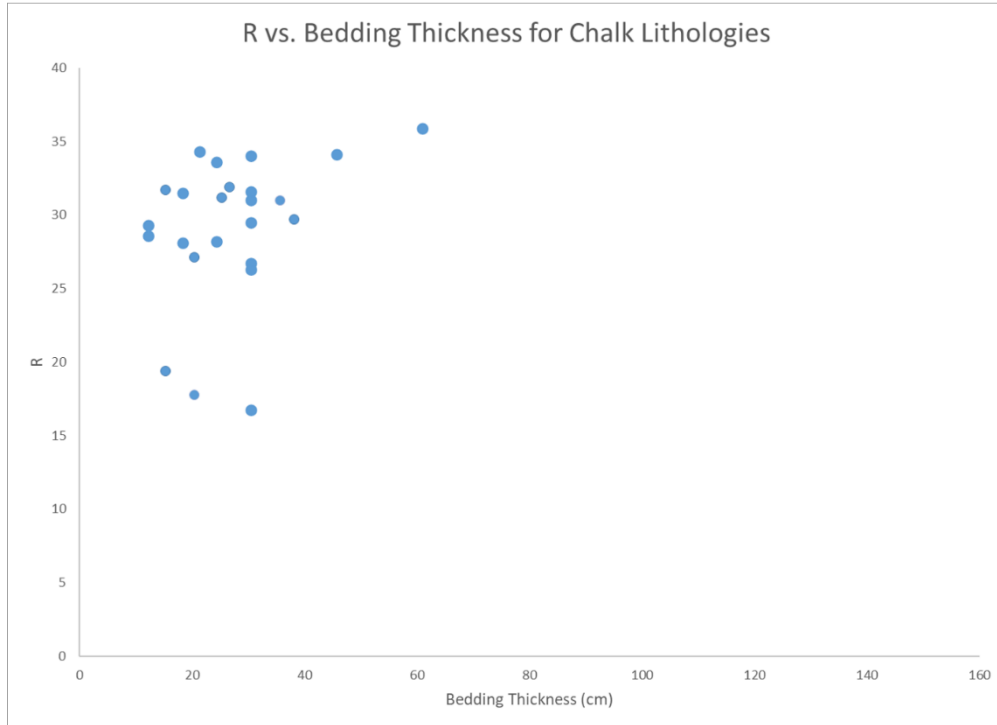
Figure 22: (Top) Relationship between rebound value (R) and bedding thickness (cm) for chalk lithology (N=27). (Bottom) Relationship between rebound value (R) and bedding thickness (cm) for marly chalk lithology (N=21).
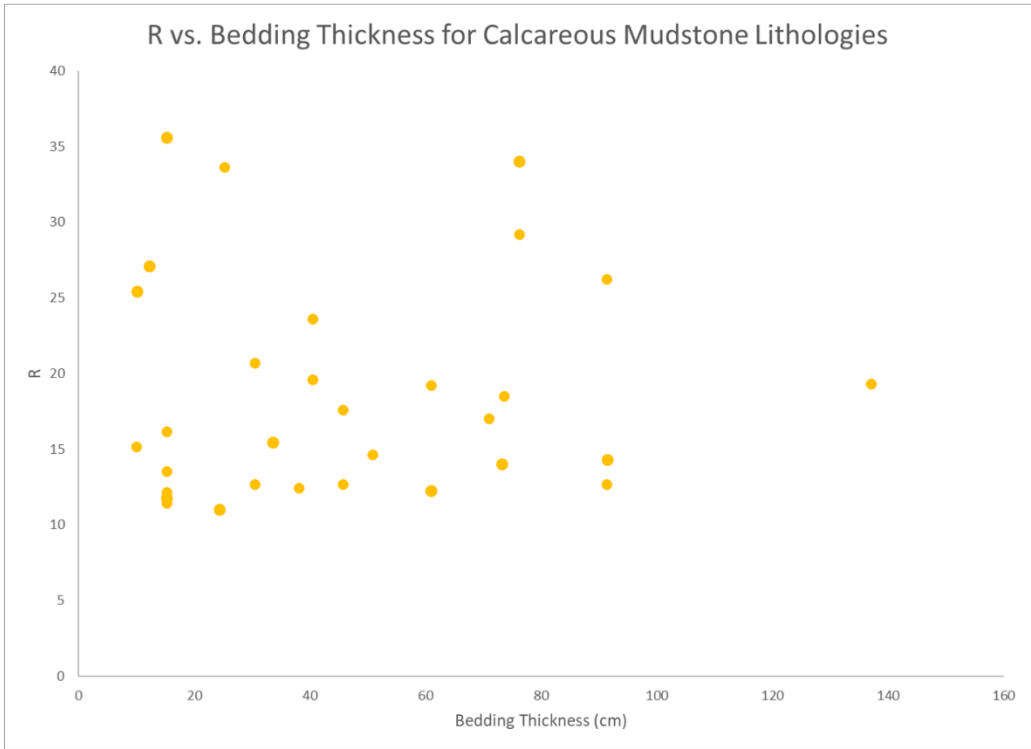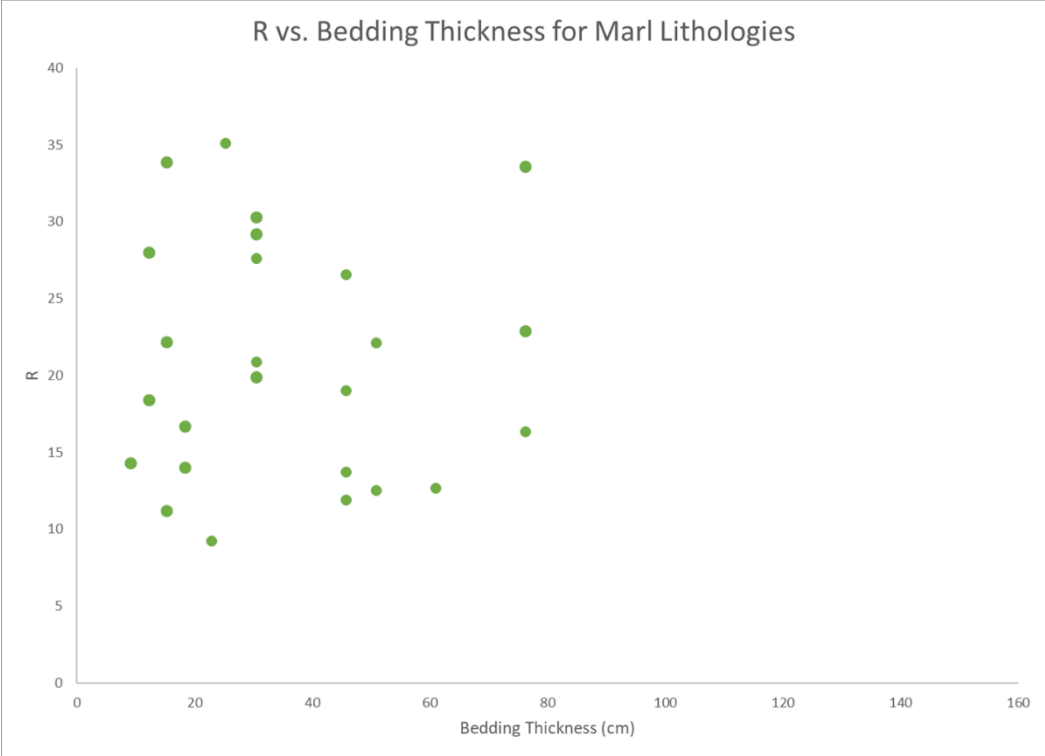
Figure 23: (Top) Relationship between rebound value (R) and bedding thickness (cm) for marl lithology (N=25). (Bottom) Relationship between rebound value (R) and bedding thickness (cm) for calcareous mudstone lithology (N=31).

Numerous studies have produced equations for correlating Schmidt hammer data with unconfined compressive strength (UCS) (e.g., Katz et al., 2000; Yilmaz and Sendir, 2002; Aydin and Basu, 2005; Bolla and Paronuzzi, 2021). Aydin and Basu (2005) provide an overview of the Schmidt hammer and compile proposed UCS correlations for a variety of lithologies and sample types. UCS correlations are typically expressed by power law, exponential, or linear functions developed for specific lithologies and sample volume (Aydin and Basu, 2005). Many correlations rely on external variables such as density and porosity. Three equations are chosen from literature to correlate R values with UCS (Figure 24). The equations selected do not rely on external variables, and have been proposed for carbonate lithologies. Equation 1, taken from Bolla and Paronuzzi (2021), is a proposed correlation for Schmidt hammer data collected *in situ* on rock outcrops of various lithologies.

$$UCS = 5.2251\text{exp}\,(0.049\text{R})$$

Equation 2, taken from Yilmaz and Sendir (2002), is a proposed correlation for marl lithologies developed by Gokceoglu (1996).

$$UCS = 0.0001 * R^{3.27}$$

Equation 3, taken from Katz et al. (2000), is a proposed correlation developed from limestone lithologies.

$$UCS = 2.21 * e^{0.07*R}$$
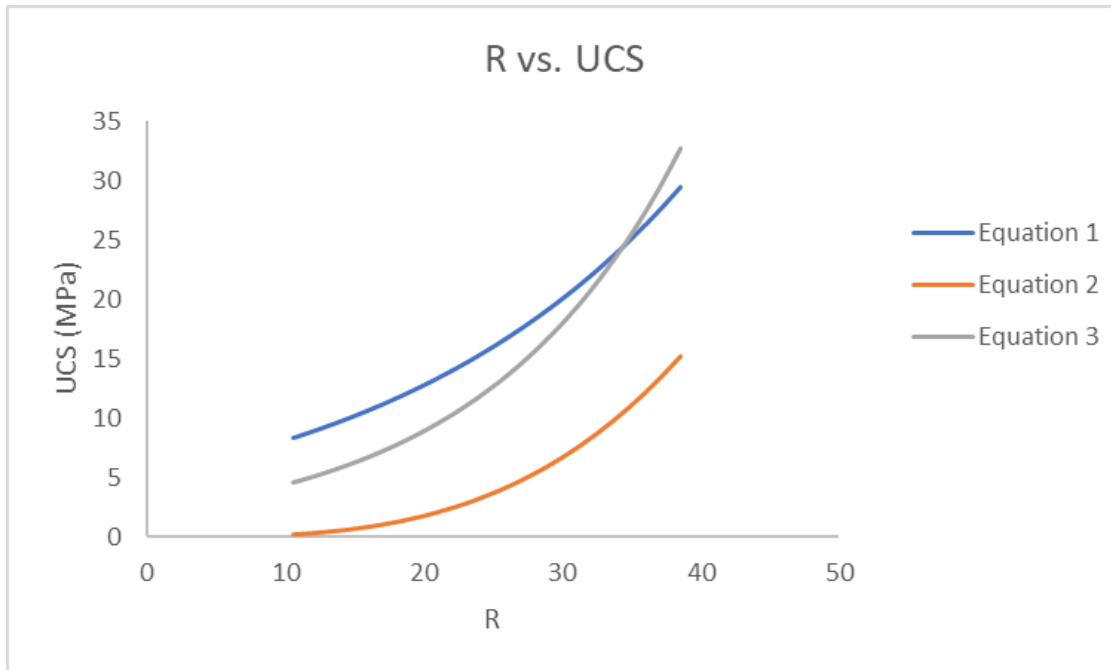
Figure 24: Relationship between rebound vale (R) and unconfined compressive strength (MPa).

III. Spectral Gamma Ray

Spectral gamma ray measurements of U (ppm), Th (ppm), and K (wt. %), and calculated gamma ray API are used to construct a spectral gamma ray profile for both outcrop sections along Ten-Mile Creek (Figures 17 and 19). Gamma ray results show API is correlated to lithology. Bentonite and calcareous mudstone layers show the sharpest spikes in gamma ray API. Bentonite lithologies show a mean API value of 45.3 and a range in values of 33.57 to 57.27. Calcareous mudstone lithologies show a range in API values of 28.42 to 60.87. Through most of the measured section, chalk and marly chalk lithologies show smooth API curves with minimal variation through the measured sections. Outliers in API values are present in carbonate-rich lithologies, leading to a wide range in API values (5.67 to 53.3). Anomalous high API values for carbonates may be a result of weathering on the outcrop

37

surface or the presence of non-carbonate impurities, such as clay minerals and iron oxides (Hladil et al., 2006).

IV.   Linear Scanline Survey Results

A total of seven linear scanline surveys, ranging in length from 15 m to 50 m, are conducted in the two sections of Ten-Mile Creek. Scanline survey locations are selected to give the best representation of fracture networks in the Ten-Mile Creek outcrop sections. Four scanline surveys are conducted within the damage zone of the faults observed, where beds are more strongly fractured and moderately folded. Specifically, scanlines 3, 4, and 6 are conducted in dipping units and may show evidence of rotation in fracture orientation. Three scanline surveys are conducted in relatively undeformed sections of the outcrop, where beds are subhorizontal and less fractured. The majority of fractures observed in Ten-Mile Creek are bedding perpendicular, Mode 1 opening fractures, commonly referred to as joints (Figure 25). Joints in Ten-Mile Creek may be sealed by calcite mineralization or open. Shear fractures dipping ~60° are also present in low abundance (Figure 26). Scanline properties, such as length, layer thickness, and rebound value are recorded (Table 1). For each scanline, linear fracture intensity and linear fracture spacing are calculated. Linear fracture intensity, or frequency, is defined as the number of fractures per unit length (m^{-1}) (Zeeb et al., 2013). Linear fracture spacing is defined as the spacing between fractures (cm) and can be calculated as the inverse of fracture intensity (Zeeb et al., 2013).

Figure 25: Fracture set consisting of Mode 1 open fractures seen in a chalk bed.

Figure 26: A conjugate set of shear fractures dipping ~60°.

Previous studies have concluded that mechanical properties influence whether an opening fracture will terminate or propagate through a bedding plane (Helgeson and Ayton, 1991; Cooke and Underwood, 2001). To investigate the relationship between fracture termination/propagation and mechanical properties all fractures are classified as bed bound and non-bed bound (Table 2) when possible. Fractures that cannot be classified due to weathering of surrounding beds are designated as not applicable. Approximately 30% of fractures measured are bed bound, and 54% of fractures are non-bed bound.

Table 1: Summary of linear scanline attributes for each scanline survey conducted in Ten-Mile Creek. Damage zone designation indicates if scanline is conducted in close proximity to fault or in a relatively undeformed bed. R is the rebound value for the bedding surface. S_L is the linear fracture spacing yielded by the scanline. I_L is the linear fracture intensity yielded by the scanline. Note linear fracture parameters have not been corrected for orientation bias.

#	SECTION	MEMBER	LENGTH (M)	THICKNESS (CM)	DAMAGE ZONE	DISTANCE FROM FAULT (M)	R	S_L (CM)	I_L (M^{-1})
1	Church	Atco	50	20.58	No	210	31.6	89.8	1.12
2	Church	Atco	50	23.96	No	210	34.3	172.4	0.58
3	Church	Atco	25	17.58	Yes	0	29.3	89.3	1.12
4	Church	Bruceville	15	21.86	Yes	0	26.7	36.9	2.71
5	Walmart	Bruceville	25	16.83	Yes	30	27.1	55.6	1.8
6	Walmart	Bruceville	15	15.6	Yes	30	28.7	42.9	2.33
7	Walmart	Bruceville	50	22.19	No	80	31.9	294.1	0.34

Table 2: Classification of fractures observed in each scanline survey. Fractures that could not be determined as bed bound or non-bed bound are designated as N/A.

#	BED BOUND	NON-BED BOUND	N/A
1	24	32	0
2	6	23	0
3	2	26	0
4	14	24	3
5	7	2	36
6	13	21	1
7	10	7	0

Three distinct fracture sets are recognized during the scanline surveys and fractures measured in each scanline survey are represented stereographically by a lower hemisphere equal area stereonet (Figures 27 and 28). Two distinct fracture sets are identified in two of the seven scanline surveys. The remaining five scanlines show outlying fractures, but do not show a distinct second fracture set. The predominant fracture set recognized in four of the scanline surveys strikes northeast-southwest and dips steeply. Average orientations at scanline 1, scanline 2, scanline 3, and scanline 5 are 220°/77°, 239°/88°, 030°/72°, and 232°/88°, respectively. A secondary fracture set at scanline 4 also has a northeast-southwest strike with an average orientation of 069°/88°. Average north-south strikes with steep dips are recognized at two of the scanline locations with average strikes and dips of 002°/90°and 193°/86° at scanlines 4 and 6, respectively. Lastly, scanline 7 shows a northwest-southeast striking average orientation of 146°/83° with similarly oriented fractures also recognized as a secondary fracture set at the scanline 5 site (average orientation of 137°/85°).
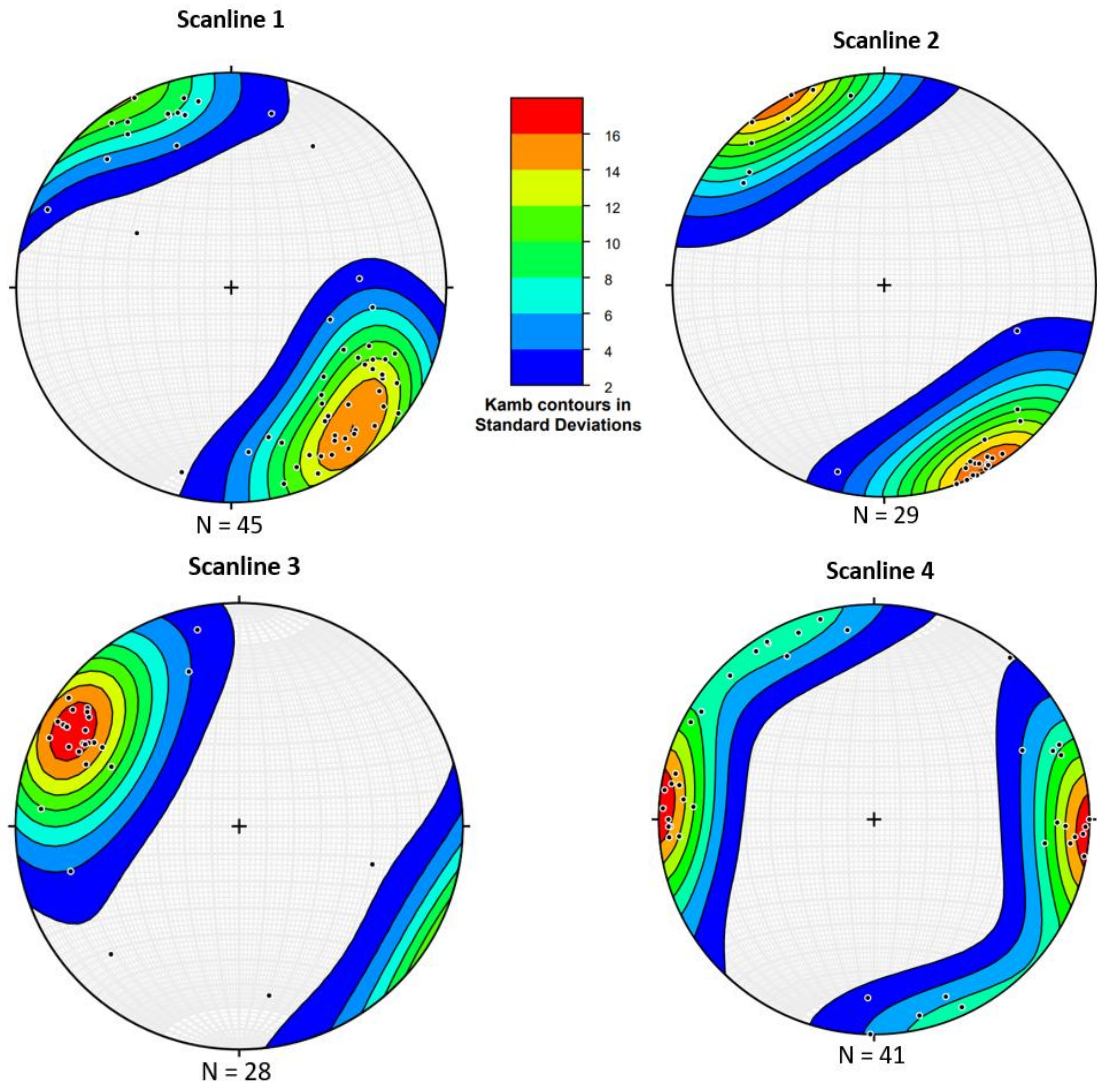
Figure 27: Lower hemisphere equal area stereographic projection of poles to fracture planes for all scanlines conducted in the Church of the Nazarene section of Ten-Mile Creek. Scanline 1 average orientation: 220°/77°. Scanline 2 average orientation: 239°/88°. Scanline 3 average orientation: 030°/71°. Scanline 4 average orientations: 002°/90° (N=28) and 069°/88° (N=13).
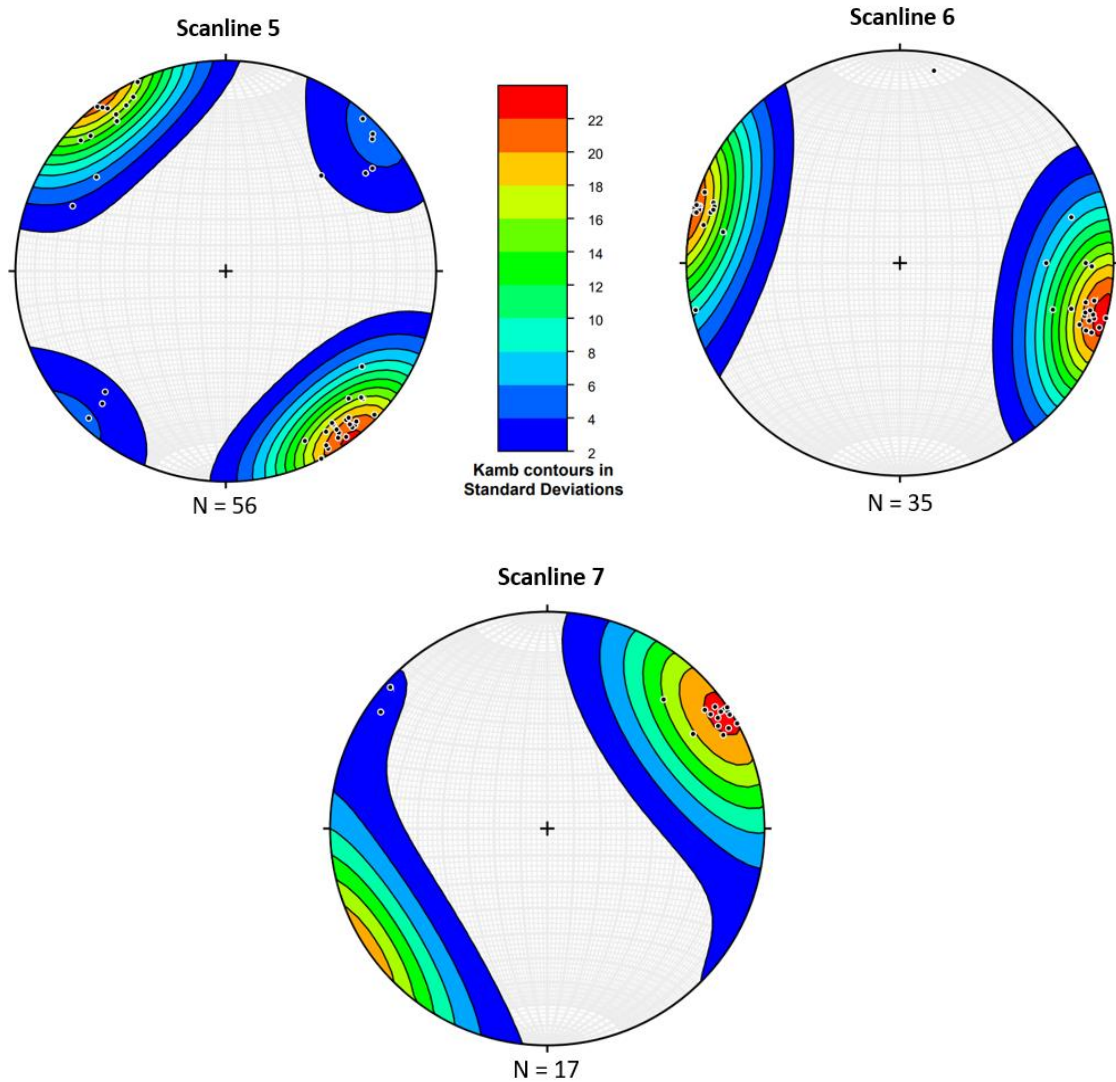
Figure 28: Lower hemisphere equal area stereographic projection of poles to fracture planes for all scanlines conducted in the Walmart section of Ten-Mile Creek. Scanline 5 average orientations: 232°/88° (N=47) and 137°/85° (N=9). Scanline 6 average orientation: 193°/86°. Scanline 7 average orientation: 146°/83°.

Because almost all measured fractures occur at an oblique angle to the scanlines, there is orientation bias in the collected data (Lacazette, 1991; Zeeb et al., 2013; Watkins et al., 2015). For each fracture set, an apparent spacing is quantified by the linear scanline and must be corrected to true spacing. Orientation bias is corrected using the method described by Lacazette (1991), which corrects the orientation bias for each individual fracture (Zeeb et al., 2013).

$$\text{Occurence} = \frac{1}{L \text{ x } \cos \propto}$$

The occurrence can be thought of as the frequency of an individual fracture, L is the length of the scanline, and α is the angle between the scanline and the pole of the fracture (Lacazette, 1991). The occurrence of all fractures in a fracture set can be summed to give the true frequency. The true spacing (S) of the fracture set can then be found by:

$$S = 1/I$$

Where *I* is the true fracture intensity. Table 3 summarizes the true fracture intensity and spacing for each fracture set measured.

Table 3: True fracture spacing and fracture intensity for each fracture set measured in Ten-Mile Creek. DZ indicates whether a scanline was conducted within the damage zone of a fault.

SCANLINE (DZ)	FRACTURE SET 1		FRACTURE SET 2	
	SPACING	INTENSITY	SPACING	INTENSITY
1 (NO)	0.79	1.27	-	-
2 (NO)	1.79	0.56	-	-
3 (YES)	0.94	1.06	-	-
4 (YES)	0.49	2.05	0.54	1.87
5 (YES)	0.67	1.48	0.62	1.61
6 (YES)	0.34	2.91	-	-
7 (NO)	0.77	1.29	-	-

Fracture spacing and fracture intensity can be compared to bedding thickness and rebound value inside and away from fault zones (Figures 29-32). Bedding thickness shows a weak positive correlation with fracture spacing (Figure 29) and a weak negative correlation with fracture intensity (Figure 30). Rebound value shows a good positive correlation (R^2 value of 0.71) with fracture spacing (Figure 31) and a moderate negative correlation with fracture intensity (Figure 32). Layers within the damage zone of faults, shown by the orange diamonds, tend to be more intensely fractured (1.06 m^{-1} to 2.91 m^{-1}), have closer fracture spacings (0.34 m to 0.94 m), and lower R values (26.7 to 29.3) when compared to layers outside the damage zone (0.56 m^{-1} to 1.29 m^{-1}, 0.77 m to 1.79 m, R=31.6 to 34.3).
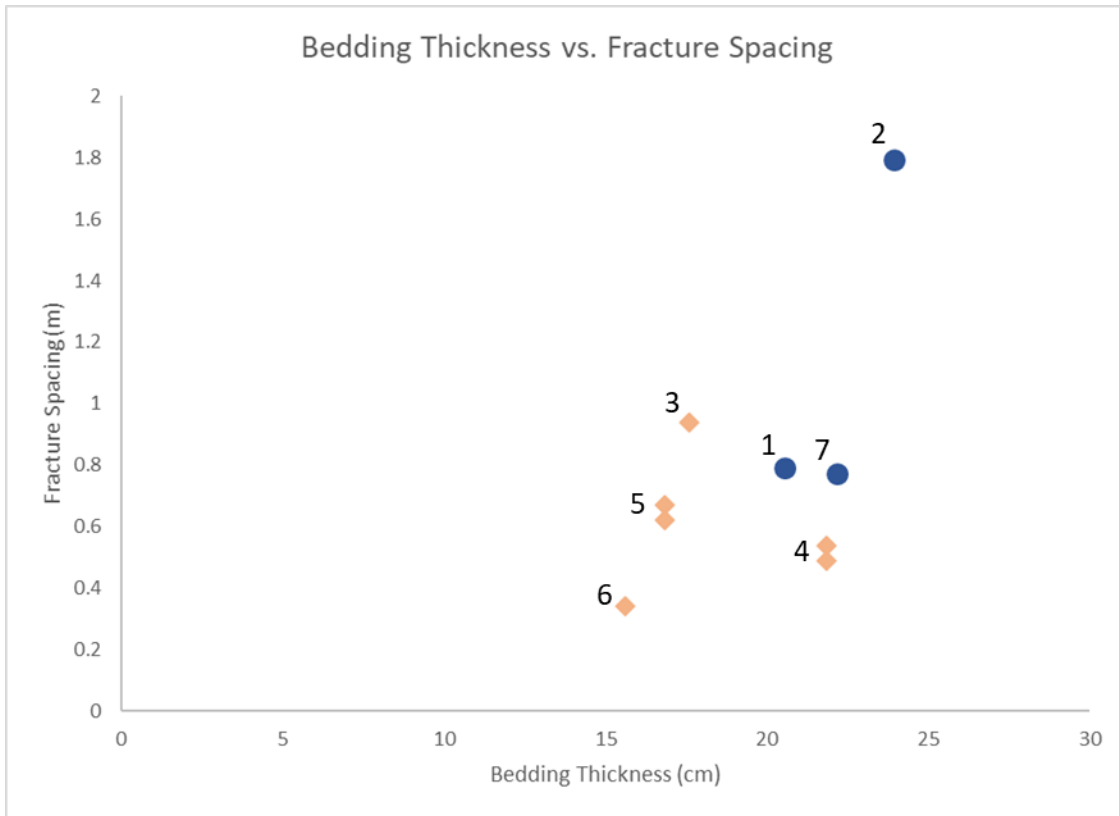
Figure 29: Relationship between bedding thickness (cm) and true fracture spacing (m). Fracture sets measured from layers within the fault damage zone are shown with orange diamonds. Fracture sets that are measured from relatively undeformed strata are shown with blue circles. Number indicates scanline.
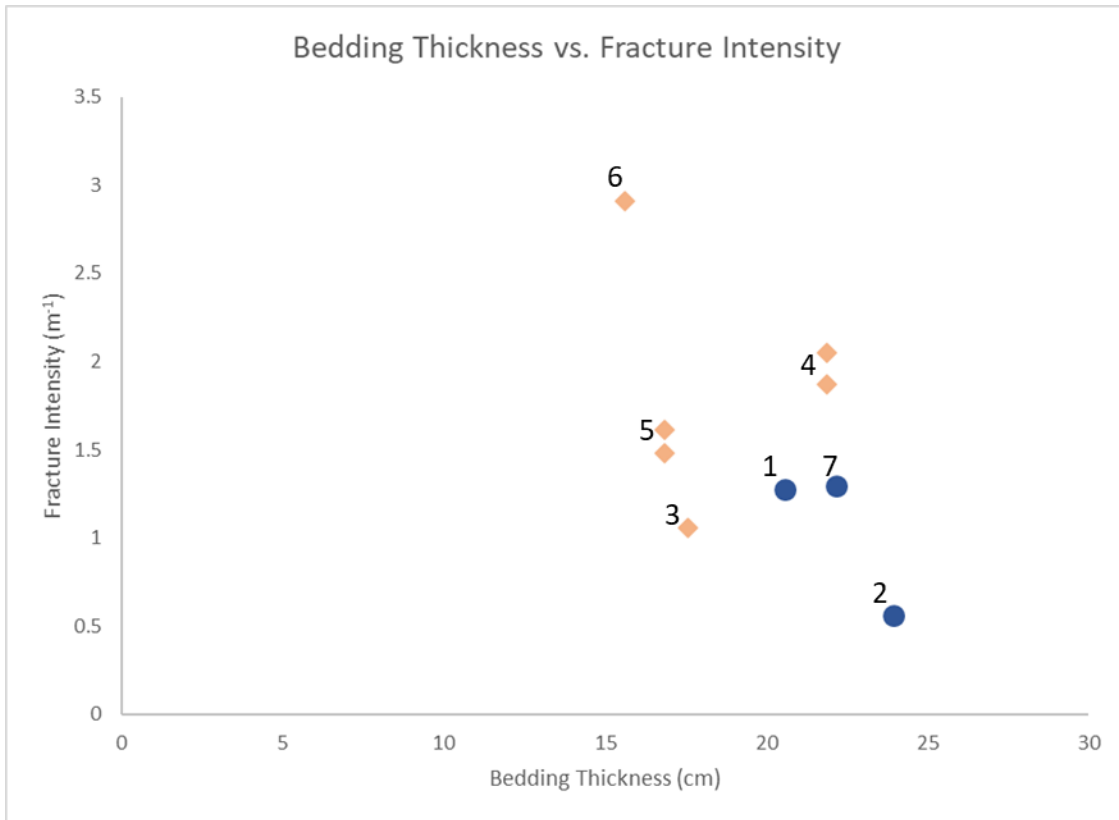
Figure 30: Relationship between bedding thickness (cm) and true fracture intensity (m^{-1}). Fracture sets measured from layers within the fault damage zone are shown with orange diamonds. Fracture sets that are measured from relatively undeformed strata are shown with blue circles. Number indicates scanline.
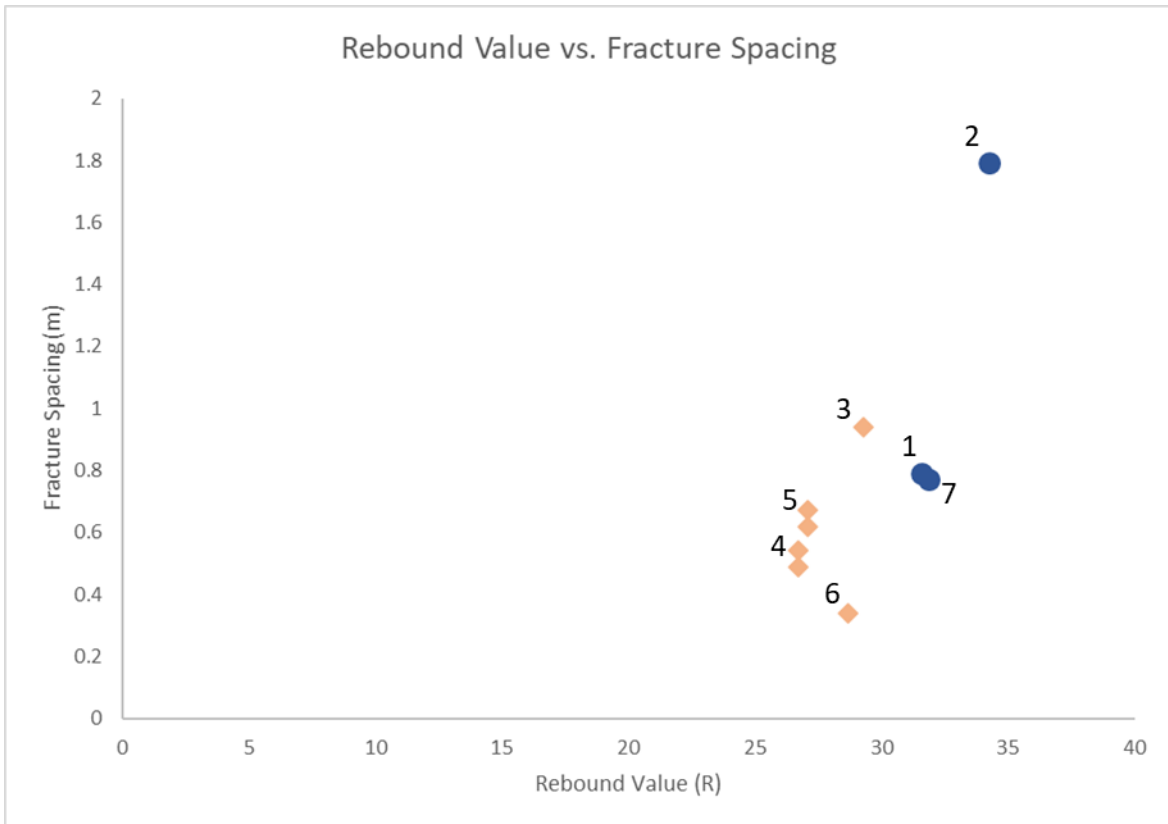
Figure 31: Relationship between rebound value (R) and true fracture spacing (m). Fracture sets measured from layers within the fault damage zone are shown with orange diamonds. Fracture sets that are measured from relatively undeformed strata are shown with blue circles. Number indicates scanline.
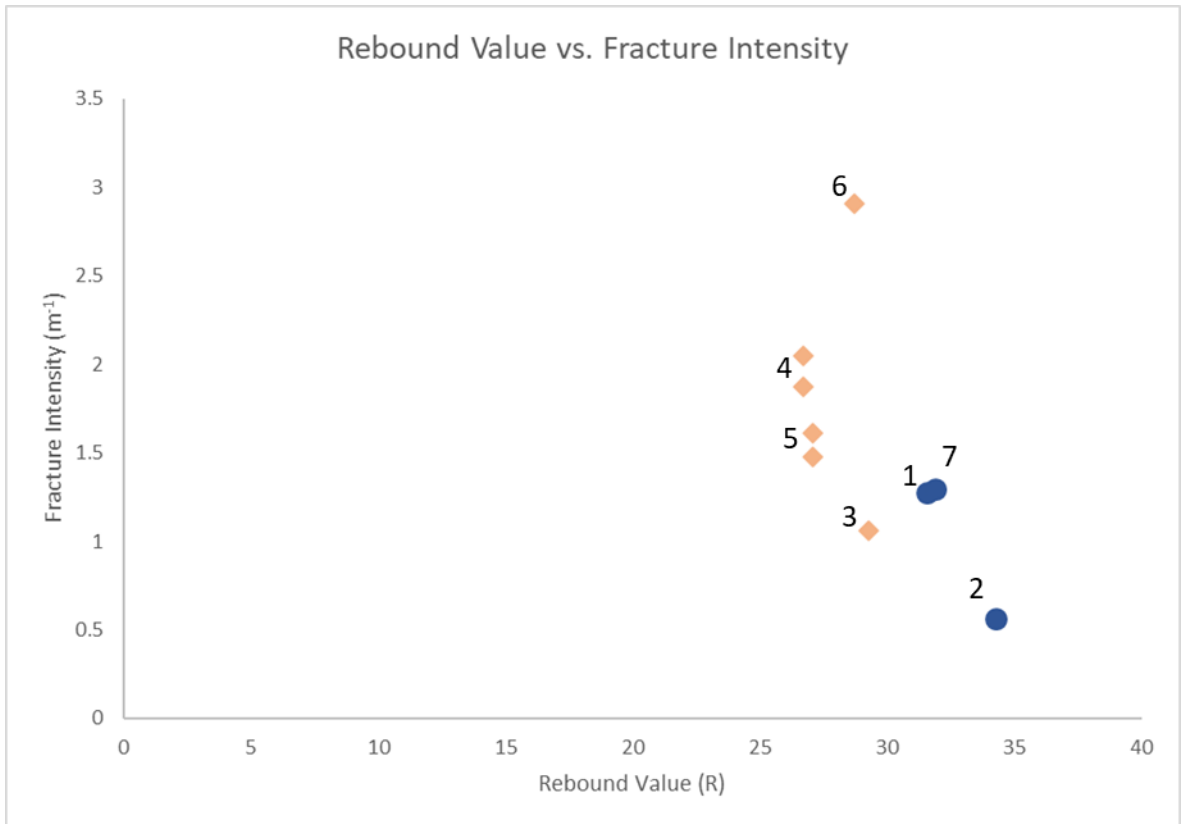
Figure 32: Relationship between rebound value (R) and true fracture intensity (m^{-1}). Fracture sets measured from layers within the fault damage zone are shown with orange diamonds. Fracture sets that are measured from relatively undeformed strata are shown with blue circles. Number indicates scanline.

Discussion

I.   Stratigraphy

The stratigraphic members of the Austin Chalk differ in lithology and competency. The Atco Member of the Austin Chalk is characterized by thick, alternating sequences of chalk and marl (Larson et al., 1995, Hancock and Walaszczyk, 2004; Gale et al., 2007; Cooper et al., 2020) and is overall described as much more competent than the Bruceville Member (Corbett et al., 1987; Ferrill et al., 2020). Lithologically, the Bruceville Member is distinguished from the Atco by thick sequences of calcareous mudstone and by the presence of pyrite nodules (Hancock and Walaszczyk, 2004; Gale et al., 2007). Previous studies support the presence of both the uppermost Atco and the Bruceville members in outcrop in Ten-Mile Creek (Gale et al., 2007). The portion north of the fault in the Church of the Nazarene section is interpreted as the Bruceville Member based on the presence of pyrite nodules and thick layers of calcareous mudstone. The portion of the section south of the fault is interpreted as the Atco Member based on lack of pyrite nodules and a large portion of the section being composed of chalk and marl. The stratigraphically highest portion of the Church of the Nazarene section (15-18.5 m; 49-61 ft) sees the appearance of thick calcareous mudstone layers again. This could suggest a transitional bedding contact from the Atco to the Bruceville Member. At least 9 m (30 ft) of the Atco Member is mapped in the Church of the Nazarene section. Based on expected thickness of the Atco, only the upper portion of this member is exposed in this section. Most of the Walmart section (0-23 m; 0-75 ft) is dominated by thick sequences of calcareous mudstone interspersed with thin beds of chalk

and consequently is interpreted as the Bruceville Member. Only the portion (23-24.7 m; 75-81 ft) south of the fault at 23 m (75 ft) is interpreted as the Atco Member.

Two of the faults present in the mapped sections of Ten-Mile Creek clearly juxtapose rocks with different lithological characteristics. Previous mapping efforts have interpreted normal faults in Ten-Mile Creek to be fault contacts between members of the Austin Chalk (Williams, 1957; Ingles, 1959; Jacobson 1961). Lithologic and structural observations indicate the faults present in both the Church of the Nazarene section and the Walmart section of Ten-Mile Creek are fault contacts between the Atco Member and the Bruceville Member of the Austin Chalk. The hanging wall of the normal fault in the Church of the Nazarene section is interpreted to be the Bruceville Member, and the footwall is interpreted to be the Atco Member. In the Walmart section, the normal fault at 23 m (75 ft) is interpreted as the contact between the Atco and Bruceville Members. In addition to these larger faults, the faults present lower in the Walmart section are contained within the Bruceville Member and show minimal displacement.

II.   Structural Analysis

The deformation styles differ between the footwall and the hangingwall of the faults in Ten-Mile Creek. Rocks in the hangingwall, consisting of the Bruceville Member, are more intensely fractured than the Atco Member (1.29 m^{-1} to 2.91 m^{-1} vs. 0.56 m^{-1} to 1.27 m^{-1}). Fracture sets are more closely spaced within the Bruceville Member (0.34 m to 0.77 m vs. 0.79 m to 1.79 m in the Atco Member). Collins (1993) describes fracture spacing ranging from 0.6 to 1.5 m, and Corbet et al. (1987) reports average fracture intensity in the middle member (Bruceville equivalent) of the Austin Chalk to be 2.0 m^{-1}. In Ten-Mile Creek,

scanline surveys conducted in the Bruceville Member yield an average fracture intensity of 1.87 m^{-1}, compared to 0.96 m^{-1} in the Atco Member. When comparing fracture networks between members with respect to fault proximity, results yield average fracture intensity values of 2.0 m^{-1} for the Bruceville Member within the damage zone, 1.29 m^{-1} for the Bruceville Member outside the damage zone, 1.06 m^{-1} for the Atco member within the damage zone, and 0.92 m^{-1} for the Atco Member outside the damage zone. Fracture spacing and intensity measured in Ten-Mile Creek are consistent with fracture networks associated with the Balcones Fault Zone described in previous studies (Corbett et al., 1987; Collins, 1993).

Mechanical stratigraphy influence normal faulting style and geometry (Ferrill et al., 2017b). Ferrill and Morris (2008) describe normal faulting processes in much of the Cretaceous section of the Balcones Fault Zone in south-central Texas. Heterolithic sequences consisting of mixed competent and incompetent strata display monoclinic folding in the footwall, a result of fault propagation folding (Ferrill and Morris, 2008). Mechanically mixed strata also display conjugate faulting and relay ramp structures (Ferrill and Morris, 2008). The Austin Chalk in Ten-Mile Creek is a mixed competent-incompetent heterolithic sequence of strong chalk and weak mudstone units. Faulted sections in Ten-Mile Creek exhibit conjugate faults, and folding in both the footwall and hangingwall. Hangingwall strata dip towards the faults in both the Church of the Nazarene section and the Walmart section, and display Mode 1 extensional fractures. Hangingwall strata dip may be explained by fault block rotation (Ferrill et al., 2017b). These features are characteristic of listric normal fault geometry (Williams and Vann, 1987; Dula, 1991; Ferrill et al., 2017b). Field

evidence suggests that the mixed competency of the strata in the section has a strong influence on the style of normal faulting in Ten-Mile Creek.

It is generally accepted that fracturing and faulting in the Austin Chalk is a result of regional extension related to subsidence in the Gulf of Mexico (Corbett et al., 1987; Wiltschko et al., 1991; Friedman and McKiernan, 1995). Previous studies have interpreted normal faults in Ellis County as the northernmost extent of the Balcones trend, and, therefore, the northernmost extent of Gulf of Mexico extension in Texas (Reaser and Collins, 1988; Collins, 1993). Collins (1993) described normal faults in Ellis County associated with the Balcones fault system with orientations in the northeast-southwest and northwest-southeast directions, he also found joints associated with faults striking in the north, northeast, east, and west directions. These findings are consistent with the faults and fractures described from Ten-Mile Creek, with the most prevalent fracture set observed with a northeast-southwest orientation. Fault orientations and fracture networks in Ten-Mile Creek are consistent with deformation associated with Balcones fault system in North Texas (Collins, 1993; Friedman and McKiernan, 1995; Ferrill and Morris, 2008; Ferrill et al., 2020). Based on these findings, the Balcones fault system can be traced further north into southern Dallas County.

III. Controls on Fracture Parameters

Relationships between fracture parameters and the physical properties of the Austin Chalk are investigated using linear scanline survey results. Studies of fracture spacing in sedimentary strata have shown that fracture type, spacing, and character are strongly influenced by lithology and mechanical bed character (McGinnis et al., 2017). McGinnis et

al. (2017) concluded that mean fracture spacing increases with bedding thickness, and that as the spacing/thickness increases, rebound value increases. Strata with lower rebound values and lower bedding thickness will show tighter fracture spacings, and be more intensely fractured (Gillespie et al., 2021). Linear scanline survey results indicate that fracture spacing in the Austin Chalk is controlled by the mechanical thickness and the rebound value (and by proxy rock strength) of the lithologic layer. As mechanical thickness and rebound value for a lithologic layer increase, so does fracture spacing, with rebound value exhibiting the strongest correlation.

Additionally, mechanical stratigraphy controls the classification (bed bound vs. non-bed bound) of fractures (Helgeson and Ayton, 1991; Gillespie et al., 1999; Cooke and Underwood, 2001; Gillespie et al., 2021). McGinnis et al. (2017) also investigated the relationship between mechanical stratigraphy, lithology, and fracture penetration, finding that chalk and limestone fractures tend to penetrate the entire bed thickness and extend into adjacent mudrocks. Approximately 30% of fractures measured in this study are bed bound, whereas 54% of fractures are non-bed bound. Notably, fractured strata from the Atco Member (scanlines 1-3) contain a higher number of non-bedbound fractures, where the overall strength of the section is higher. Cooke and Underwood (2001) note that a fracture is more likely to terminate at a very weak interface, rather than an interface of high or moderate strength. Ductile layers, like mudstone, represent weak interfaces, which tend to impede the vertical propagation of fractures (Cooke and Underwood, 2001; Gillespie et al, 2021). In contrast to the Atco Member, fractured strata in the Bruceville Member (scanlines 4-7) contain a higher number of bed-bound fractures. However, surrounding mudstone units may

be weathered away in outcrop, making classification of fractures in these strata more difficult.

Conclusion

Structural and mechanical analysis of the Austin Chalk outcrops in Ten-Mile Creek show normal faulting and fracture networks related to uniform extension typically seen in heterolithic carbonate-mudstone sequences. Schmidt hammer results yield rebound values ranging from 9 to 35.9, and show that rebound value in outcrop, a proxy for *in situ* rock strength, is strongly influenced by lithology. The Atco Member consisting of alternating sequences of chalk and marl is stronger than the Bruceville Member consisting of thin chalk beds between thick beds of calcareous mudstone. Three fracture sets are observed consisting predominately of Mode 1 opening fractures with northeast-southwest, north-south, and northwest-southeast strikes. Analysis of fracture networks in the Austin Chalk in Ten-Mile Creek yield fracture spacing values ranging from 0.34 m to 1.79 m and fracture intensity values ranging from 0.54 m^{-1} to 2.91 m^{-1}. Fracture spacing shows a positive correlation with rebound value, and the outcrop sections are more intensely fractured in close proximity to normal faulting. Normal faulting in Ten-Mile Creek juxtaposes rocks of the Atco and Bruceville Members. Results are consistent with fracture networks associated with normal faulting related to the Balcones Fault Zone described in Ellis County, and, therefore, the trend of the Balcones Fault Zone extends into southern Dallas County.

Bibliography

Aydin, A., Basu, A., 2005, The Schmidt hammer in rock material characterization:

    Engineering Geology, vol. 81, pg. 1 – 14

Basu, A., Aydin, A., 2004, A method for normalization of Schmidt hammer rebound values:

    International Journal of Rock Mechanics & Mining Sciences, vol. 41 pg. 1211 – 1214

Bolla, A., Paronuzzi, P., 2021, UCS field estimation of intact rock using the Schmidt

    hammer: A new empirical approach: IOP Conference Series: Earth and

    Environmental Science, vol. 833, pg. 1 – 8

Callarotti, G. F., Millican, S. F., 2012, Openhole Multistage Hydraulic Fracturing Systems

    Expand the Potential of the Giddings Austin Chalk Field: Society of Petroleum

    Engineers, 152402

Collins, E. W., 1993, Fracture zones between overlapping en echelon fault strands: outcrop

    analogs within the Balcones fault zone, central Texas: Gulf Coast Association of

    Geological Societies, pg. 77 – 85

Collins, J. G., 1997, Characteristics and origin of the Cedar Hill Bentonite bed, lower Austin

    Chalk, Dallas County vicinity, MS: University of Texas at Arlington

Cooke, M. L., Underwood, C. A., 2001, Fracture termination and step-over at bedding

    interfaces due to frictional slip and interface opening: Journal of Structural Geology,

    vol. 23, pg. 223 – 238

Cooper, J. R., Godet, A., Pope, M. C., 2020, Tectonic and eustatic impact on depositional

     features in the upper Cretaceous Austin Chalk Group of south-central Texas, USA:

     Sedimentary Geology, 401, pg. 1 – 17

Corbett, K., Friedman, M., Spang, J., 1987, Fracture Development and Mechanical

     Stratigraphy of Austin Chalk, Texas: AAPG Bulletin, vol. 71, no. 1, pg. 17 – 28

Damholt, T., Surlyk, F., 2004, Laminated–bioturbated cycles in Maastrichtian chalk of the

     North Sea: oxygenation fluctuations within the Milankovitch frequency band:

     Sedimentology, vol. 51, pg. 1323 – 1342

Denne, R. A., 2018, Plankton: Encyclopedia of Petroleum Geoscience, pg. 1 – 11

Dravis, J. J., 1980, Sedimentology and diagenesis of the Upper Cretaceous Austin Chalk

     formation, south Texas and northern Mexico, PhD: Rice University, University

     Microfilms International

Dula, Jr., W. F., 1991, Geometric Models of Listric Normal Faults: AAPG Bulletin, vol. 75,

     no. 10, pg. 1609 – 1625

Dunham, R. J., 1962, Classification of carbonate rocks according to depositional texture, in

     W. E. Ham, ed., Classification of carbonate rocks: AAPG Memoir 1, p. 108 – 121.

Eldrett, J. S., Ma, C., Bergman, S. C., Ozkan, A., Minisini, D., Lutz, B., Jackett, S.,

     Macaulay, C., Amy, E. K., 2015, Origin of limestone–marlstone cycles: Astronomic

     forcing of organic-rich sedimentary rocks from the Cenomanian to early Coniacian of

     the Cretaceous Western Interior Seaway, USA: Earth and Planetary Science Letters,

     423, pg. 98 – 113

Ferrill, D. A., Morris, A. P., 2008, Fault zone deformation controlled by carbonate
mechanical stratigraphy, Balcones fault system, Texas: AAPG Bulletin, vol. 92, no. 3,
pg. 359 – 380

Ferrill, D. A., Morris, A. P., McGinnis, R. N., Smart, K. J., Ward, W. C., 2011, Fault zone
deformation and displacement partitioning in mechanically layered carbonates: The
Hidden Valley fault, central Texas: AAPG Bulletin, vol. 95, no. 8, pg. 1383 – 1397

Ferrill, D. A., Evans, M. A., McGinnis, R. N., Morris, A. P., Smart, K. J., Wigginton, S. S.,
Gulliver, K. D. H., Lehrmann, D., Zoeten, E. D., Sickmann, Z., 2017a, Fault zone
processes in mechanically layered mudrock and chalk: Journal of Structural Geology,
vol. 97, pg. 118 – 143

Ferrill, D. A., Morris, A. P., McGinnis, R. N., Smart, K. J., Wigginton, S. S., Hill, N. J.,
2017b, Mechanical stratigraphy and normal faulting: Journal of Structural Geology,
vol. 94, pg. 275 – 302 13

Ferrill, D. A., Evans, M. A., McGinnis, R. N., Morris, A. P., Smart, K. J., Lehrmann, D.,
Gulliver, K. D. H., Sickmann, Z., 2020, Fault zone processes and fluid history in
Austin Chalk, southwest Texas: AAPG Bulletin, vol. 104, no. 2, 245 – 283

Friedman, M., McKiernan, D. E., 1995, Extrapolation of Fracture Data from Outcrops of the
Austin Chalk in Texas to Corresponding Petroleum Reservoirs at Depth: Journal of
Canadian Petroleum Technology, vol. 34, no. 8, pg. 43 – 49

Gale, A. S., Kennedy, W. J., Lees, J. A., Petrizzo, M. R., Walaszczyk, I., 2007, An integrated
study (inoceramid bivalves, ammonites, calcareous nannofossils, planktonic
foraminifera, stable carbon isotopes) of the Ten Mile Creek section, Lancaster, Dallas

County, north Texas, a candidate Global boundary Stratotype Section and Point for the base of the Santonian Stage: Acta Geologica Polonica, vol. 57, no. 2, pg. 113 – 160

Gale, A. S., Hancock, J. M., Kennedy, W. J., Petrizzo, M. R., Lees, J. A., Walaszczyk, I., Wray, D. S., 2008, An integrated study (geochemistry, stable oxygen and carbon isotopes, nannofossils, planktonic foraminifera, inoceramid bivalves, ammonites and crinoids) of the Waxahachie Dam Spillway section, north Texas: a possible boundary stratotype for the base of the Campanian Stage: Cretaceous Research, 29, pg. 131 – 167

Galloway, W. E., 2008. Depositional Evolution of the Gulf of Mexico Sedimentary Basin: Sedimentary Basins of the World, vol. 5, pg. 505 – 549

Gillespie, P. A., Johnston, D. A., Loriga, M. A., McCaffrey, K. J W., Walsh, J. J., Watterson, J., 1999. Influence of Layering on Vein Systematics in Line Samples: Geological Society, London, Special Publications, 155, pg. 35 – 56

Gillespie, P. A., Holdsworth, R. E., Long, D., Williams, A., Gutmanis, G. C., 2021, Introduction: geology of fractured reservoirs: Journal of the Geological Society, vol. 178, pg. 1 – 12

Gokceoglu, C., 1996. Schmidt sertlik cßekici kullanılarak tahminedilen tek eksenli basıncßdayanımı verilerinin gu ̈venilirlig ̆iu ̈zer-ine bir deg ̆erlendirme. Jeol. Mu ̇hendislig ̆i 48, 78–81(InTurkish).

Hancock, J. M., Walaszczyk, I., 2004, Mid-Turonian to Coniacian changes of sea level around Dallas, Texas: Cretaceous Research, vol. 25, pg. 459 – 471

Helgeson, D. E., Ayton, A., 1991, Characteristics of joint propagation across layer interfaces in sedimentary rocks: Journal of Structural Geology, vol. 13, no. 8, pg. 897 – 911

Hladil, J., Gersl, M., Strnad, L., Frana, J., Langrova, A., Spisiak, J., 2006, Stratigraphic variation of complex impurities in platform limestones and possible significance of atmospheric dust: a study with emphasis on gamma-ray spectrometry and magnetic susceptibility outcrop logging (Eifelian-Frasnian, Moravia, Czech Republic): International Journal of Earth Science, 95, pg. 703 – 723

Hovorka, S. D., Nance, H. S., 1994, Dynamic Depositional and Early Diagenetic Processes in a Deep-Water Shelf Setting, Upper Cretaceous Austin Chalk, North Texas: Transactions of the Gulf Coast Association of Geological Societies, vol. XLIV, pg. 269 – 276

Ingles, J. J. C., 1959, Geology of the Lancaster Quadrangle of Dallas and Ellis counties, Texas: Field and Laboratory, vol. XXVII, pg. 1 – 10

Jacobson, J. M., 1961, Vertical Distribution of Foraminifera in the Lower Chalk Member of the Austin Formation, Southern Dallas County, Texas: Journal of the Graduate Research Center, pg. 179 – 187

Katz, O., Reches, Z., Roegiers, J. C., 2000, Evaluation of mechanical rock properties using a Schmidt Hammer: International Journal of Rock Mechanics and Mining Sciences, vol. 37, pg. 723 – 728

Larson, P., Morin, R., Larson, A., Clarke, B.,1995. Sequence Stratigraphy and cyclicality of Lower Austin/Upper Eagle Ford outcrops (Turonian-Coniacian), Dallas County,

Texas: American Association of Petroleum Geologists Southwest Section Convention Guidebook Field Trip #1, pg. 1 – 14

Lacazette, A., 1991, A stereographic technique for the reduction of scanline survey data of geologic features: Computers and Geosciences, vol. 17, pg. 445 – 463

Longman, M. W., Luneau, B. A., Landon, S. M., 1998, Nature and Distribution of Niobrara Lithologies in the Cretaceous Western Interior Seaway of the Rocky Mountain Region: The Mountain Geologist, vol. 35, no. 4, pg. 1137 – 170

Loucks, R. G., Larson, T. E., Zheng, C. Y. C., Zahm, C. K., Ko, L. T., Sivil, J. E., Sheng, P., Ruppel, S. C., Ambrose, W. A., 2020, Geologic characterization of the type core section for the Upper Cretaceous Austin Chalk Group in southern Texas: A combination fractured and unconventional reservoir: AAPG Bulletin, vol. 104, no. 10, pg. 2209 – 2245

Lundquist, J. J., 2000, Foraminiferal Biostratigraphic and Paleooceanographic Analysis of the Eagle Ford, Austin, and Lower Taylor Groups (Middle Cenomanian through Lower Campanian) of Central Texas, PhD: University of Texas at Austin

McClave, G. A, 2014, Correlation of Rebound-Hammer Rock Strength With Core and Sonic Log-Derived Mechanical Rock Properties in Cretaceous Niobrara and Frontier 14 Formation Cores, Piceance Basin, Colorado: Unconventional Resources Technology Conference, 1921941, pg. 847 – 863

McGinnis, R. N., Ferrill, D. A., Morris, A. P., Smart, K. J., Lehrmann, D., 2017, Mechanical stratigraphic controls on natural fracture spacing and penetration: Journal of Structural Geology, vol. 95, pg. 160 – 170

Narr, W., Suppe, J., 1991, Joint spacing in sedimentary rocks: Journal of Structural Geology, vol. 13, no. 9, pg. 1037 – 1048

Norton, G. H., 1965, Surface Geology of Dallas County, The Geology of Dallas County: Dallas Geological Society, plate 1

Phelps, R. M., Kerans, C., Loucks, R. G., Da Gama, R. O. B. P., Jeremiah, J., Hull, D., 2014, Oceanographic and eustatic control of carbonate platform evolution and sequence stratigraphy on the Cretaceous (Valanginian–Campanian) passive margin, northern Gulf of Mexico: Sedimentology, vol. 61, pg. 461 – 496

Priest, S. D., Hudson, J. A., 1981, Estimation of Discontinuity Spacing and Trace Length Using Scanline Surveys: International Journal of Rock Mechanics, Mining Science, and Geomechanics, vol. 18, pg. 183 – 197

Radiation Solutions Inc., 2019, RS-125/230 User Manual: Radiation Solutions Inc.

Reaser, D. F., 1961, Balcones fault system: its northeast extent: Geological Notes, pg. 1759 – 1762

Reaser, D. F., Collins, E. W., 1988, Style of faults and associated fractures in Austin Chalk, northern extension of the Balcones fault zone, central Texas: Gulf Coast Association of Geological Societies, vol. XXXVIII, pg. 267 – 276

Verwaal W., Mulder, A., 1993, Estimating Rock Strength with the Equotip Hardness Tester: International Journal of Rock Mechanics, Mining Science, and Geomechanics, vol. 30, no. 6, pg. 659 – 662

Watkins, H., Bond, C. E., Healy, D., Butler, R. W. H., 2015, Appraisal of fracture sampling
    methods and a new workflow to characterize heterogeneous fracture networks at
    outcrop: Journal of Structural Geology, vol. 72, pg. 67 – 82

Weeks, A. W., 1945, Balcones, Luling, and Mexia Fault Zones in Texas: AAPG Bulletin,
    vol. 29, no. 12, pg. 1733 – 1737

Williams, T. E., 1957, Correlation of Insoluble Residues in the Austin Chalk of southern
    Dallas County, Texas: Field and Laboratory, vol. XXV, pg. 37 – 45

Williams, G., Vann, I., 1987, The geometry of listric normal faults and deformation in their
    hanging walls: Journal of Structural Geology, vol. 9, no. 7, pg. 789 – 795

Wiltschko, D. V., Corbett, K. P., Friedman, M., Hung, J., 1991, Predicting fracture
    connectivity and intensity within the Austin Chalk form outcrop fracture maps and
    scanline data: Gulf Cost Association of Geological Societies, vol. XLI, pg. 702 – 718

Yilmaz, I., Sendir, H., 2002, Correlation of Schmidt hammer hardness with unconfined
    compressive strength and Young's modulus in gypsum from Sivas (Turkey):
    Engineering Geology, vol. 66, pg. 211 – 219

Zahm, C. K., Enderlin, M., 2010, Characterization of Rock Strength in Cretaceous Strata
    along the Stuart City Trend, Texas: Gulf Coast Association of Geological Societies
    Transactions, v. 60, pg. 693 – 702

Zeeb, C., Gomez-Rivas, E., Bons, P. D., Blum, P., 2013, Evaluation of sampling methods for
    fracture network characterization using outcrops: AAPG Bulletin, vol. 97, no. 9, pg.
    1545 – 1566

VITA

Personal Background	Patrick Carter Lewis
	Born September 26, 1997, Fort Worth, Texas
	Son of Patrick Lewis and Leslee Lewis
Education	Bachelor of Science in Geology, 2020
	Texas Tech University, Lubbock, Texas
	Master of Science in Geology, 2022
	Texas Christian University, Fort Worth, Texas
Experience	Mud Logger, 2018
	Riley Geological Consultants, Slaton, Texas

ABSTRACT

MECHANICAL STRATIGRAPHY AND FAULT ZONE DEFORMATION OF THE
AUSTIN CHALK IN TEN-MILE CREEK, DESOTO, TEXAS

By Patrick Carter Lewis, M.S., 2022
Department of Geological Sciences
Texas Christian University

Dr. Helge Alsleben – Associate Professor of Geology

The Austin Chalk is a rhythmically bedded sequence of chalk and marl that represents

carbonate deposition in the ancestral Gulf of Mexico during the Upper Cretaceous. The

Austin Chalk differs from other chalk deposits due to its relatively high abundance of clay

and volcanic ash. Outcrops of the formation stretch from north-central Texas to west Texas.

This study presents a structural analysis from two sections along Ten-Mile Creek in DeSoto,

Texas, where deformation of the Austin Chalk is characteristic of normal faulting in platform

carbonate sequences. Outcrop studies provide the most complete view of a lithological unit.

Analysis of fracture networks in outcrop provide a key insight into deformation of rock

formations in the subsurface that cannot be gathered from subsurface data. Results show that

fracture parameters correlate with mechanical properties and lithology, and that deformation

in Ten-Mile Creek is consistent with that related to the Balcones Fault Zone.